

Evidence for strong intracluster magnetic fields in the early Universe

J. XU^{1,2} AND J. L. HAN^{1,2,3}

¹National Astronomical Observatories, Chinese Academy of Sciences, A20 Datun Road, Chaoyang District, Beijing 100101, China

²CAS Key Laboratory of FAST, NAOC, Chinese Academy of Sciences

³School of Astronomy and Space Sciences, University of Chinese Academy of Sciences, Beijing 100049, China

ABSTRACT

The origin of magnetic fields in clusters of galaxies is still a matter of debate. Observations for intracluster magnetic fields over a wide range of redshifts are crucial to constrain possible scenarios for the origin and evolution of the fields. Differences of Faraday rotation measures (RMs) of an embedded double radio sources, i.e. a pair of lobes of mostly Fanaroff–Riley type II radio galaxies, are free from the Faraday rotation contributions from the interstellar medium inside the Milky Way and the intergalactic medium between radio galaxies and us, and hence provide a novel way to estimate average magnetic field within galaxy clusters. We have obtained a sample of 627 pairs whose RMs and redshifts are available in the most updated RM catalogues and redshift databases. The RM differences of the pairs are derived. The statistically large RM differences for pairs of redshifts $z > 0.9$ indicate that intracluster magnetic fields is as strong as about 4 μG . Such strong magnetic fields in the intracluster medium at the half age of the Universe, comparable to intracluster field strength in nearby galaxy clusters, pose a challenge on the theories for origin of cosmic magnetic fields.

Keywords: galaxies: magnetic fields — galaxies: clusters: intracluster medium — radio continuum: galaxies

1. INTRODUCTION

In the past decades, magnetic fields in galaxy clusters have been observed and studied (see review of Han 2017; Carilli & Taylor 2002; Govoni & Feretti 2004; Ferrari et al. 2008; Feretti et al. 2012). The magnetic fields are crucial for a comprehensive understanding of radio emission from the diffuse intracluster medium (ICM). The presence of diffuse radio halos and radio relics in galaxy clusters is the direct evidence for magnetic fields in the ICM (e.g. Giovannini et al. 2009; van Weeren et al. 2010). Under the minimum energy hypothesis or equipartition approach, magnetic fields permeating the ICM are roughly estimated from the radio emission intensity maps with a strength of a few micro-Gauss (e.g. Govoni & Feretti 2004).

Statistical study of Faraday rotation measures (RMs) of radio sources within or behind galaxy clusters is an alternative way to investigate magnetic fields in galaxy clusters (e.g. Kim et al. 1991; Clarke et al. 2001; Govoni et al. 2010; Bonafede et al. 2010, 2013; Pratley et al. 2013; Böhringer et al. 2016). When a linearly polarized electromagnetic wave signal travels through a magnetized plasma,

the plane of polarization is rotated by an angle $\Delta\psi$ proportional to the wavelength squared λ^2 , i.e.

$$\Delta\psi = \psi - \psi_0 = \text{RM} \cdot \lambda^2, \quad (1)$$

where ψ and ψ_0 are the measured and intrinsic polarization angle, and RM is the rotation measure which is an integrated quantity of the product of the thermal electron density n_e and magnetic field strength B from the source to us, most effectively probing the fields along the line of sight. For a polarized radio source at redshift z_s , RM is expressed by

$$\text{RM} = 812 \int_{\text{source}}^{\text{us}} n_e B \cdot dl = 812 \int_{z_s}^{\text{us}} \frac{n_e(z) B_{||}(z)}{(1+z)^2} \frac{dl}{dz} dz. \quad (2)$$

The electron density n_e is in cm⁻³, the magnetic field is a vector B (and magnetic field along the line of sight $B_{||}$) in units of μG , and dl is the unit vector along the light path towards us in units of kpc. The comoving path increment per unit redshift $\frac{dl}{dz}$ is in kpc and $(1+z)^2$ reflects the change of wavelength at redshift z over the path transformed to the observer's frame.

The observed rotation measure RM_{obs} , is a sum of the foreground Galactic RM (GRM) from the Milky Way, the rotation measure from intergalactic medium RM_{IGM} and in-

trinsic to the source RM_{in} i.e.

$$\text{RM}_{\text{obs}} = \text{GRM} + \text{RM}_{\text{IGM}} + \text{RM}_{\text{in}}. \quad (3)$$

When studying RMs of sources at a cosmological distance, one has to account RM contributions from all kinds of the intervening medium along the line of sight. For most extragalactic radio sources, the foreground Galactic RM is the dominant contribution. If the foreground GRM is not assessed properly, it is impossible to get small extragalactic contributions. There have been many efforts to investigate the foreground GRM (e.g. Han et al. 1997; Oppermann et al. 2012; Xu & Han 2014a; Oppermann et al. 2015). RM values intrinsic to a radio source (RM_{in}) at a redshift of z_s are reduced by a factor $(1 + z_s)^{-2}$ due to change of λ when the values are transformed to the observer's frame. The typical distribution of source-intrinsic RMs of distant quasar-like sources is only several rad m⁻² (Banfield et al. 2014). The RMs from the intergalactic medium RM_{IGM} may have several contributors, such as rotation measures from the cosmic webs, intervening galaxy halos and intracluster medium on the line of sight. The rotation measure from the cosmic webs might be traced by Ly α forest, and there have been some simulations on their contribution (e.g. Blasi et al. 1999; Akahori & Ryu 2010, 2011; Pshirkov et al. 2016). It is very small ($\sim 1\text{--}2$ rad m⁻²) that it hardly be detected from present available data (Xu & Han 2014b; O'Sullivan et al. 2019, 2020). The excess of rotation measure from galaxy halos or protogalactic environments has been studied by intervening absorbers like Mg II absorption lines (e.g. Bernet et al. 2008; Farnes et al. 2014, 2017). Joshi & Chand (2013) and Malik et al. (2020) obtained an increase in the distribution deviation of around 8 rad m⁻² for quasars with Mg II absorption lines. Statistics of RMs of polarized radio sources located inside or behind galaxy clusters (e.g. Kim et al. 1991; Clarke et al. 2001; Govoni et al. 2010; Bonafede et al. 2010, 2013; Pratley et al. 2013; Böhringer et al. 2016) show the RM excess for the contributions from the intracluster medium with an amplitude from a few to a few tens of rad m⁻² (Xu & Han 2014b; Govoni et al. 2010; Clarke et al. 2001).

It is now well established that the magnetic fields are ubiquitous in the ICM (e.g. Carilli & Taylor 2002). The intracluster magnetic fields are dominated by turbulent fluctuations over a range of scales. The field strength decreases from the central regions to the outskirts. The spatial power spectrum is well represented by a Kolmogorov power spectrum (Bonafede et al. 2010). Turbulent magnetic fields with a coherence length of a few kpc are indicated by RM dispersion studies of polarized radio sources (e.g. Kim et al. 1991; Govoni et al. 2010) and found in both relaxed clusters and merging clusters regardless of dynamic states (Clarke et al. 2001; Böhringer et al. 2016; Stasyszyn & de los Rios 2019).

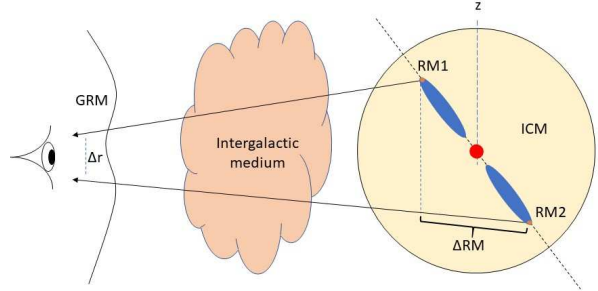


Figure 1. A schematic diagram showing a pair of lobes from a FR II radio galaxy with observed RMs on each side (RM1 and RM2, respectively). The RMs of the pair with such a small angular separation (Δr) of an order of arcminutes have almost the same Galactic contributions (in general coherent from several degrees at low Galactic latitudes to tens of degrees at high Galactic latitudes) and the same intergalactic contributions in front of the lobes. Therefore the RM difference (ΔRM) between the two lobes are the best probes for the magnetic properties of the ICM.

Coherent rotation measures of radio relics reveal large-scale (>100 kpc) compressed magnetic fields (Owen et al. 2014; Kierdorf et al. 2017). The organized magnetic fields are responsible for systematic RM gradient over lobes of radio galaxies (e.g. Taylor & Perley 1993). The ordered net magnetic fields can be considered as the large-scale fluctuations at the outer scale of turbulent magnetic fields where the energy is injected (Vacca et al. 2010). The magnetic fields close to the center of galaxy clusters are more disturbed and tangled with a strength of a few micro-Gauss while those near the outskirts are more representative for the large-scale fluctuation component with a field strength of an order of magnitude smaller (Ryu et al. 2008).

The RM difference of a pair of lobes from an embedded FR II radio galaxy (Fanaroff & Riley 1974) are the best probes for the magnetic fields in the ICM and their redshift evolution, because both the foreground Galactic RM and the RM contributions on the way to the cluster in all intervening galactic and intergalactic medium can be diminished, as depicted in Figure 1. The real physical pair of lobes are the bulk of radio emission from a galaxy on opposite sides, formed when central active galactic nuclei produce two opposite collimated jets that drive relativistic electrons running in magnetic fields into the lobes to generate synchrotron emission (Blandford & Rees 1974). The environs of the host galaxy must be rich of gas. The jets travel through the interstellar medium of the host galaxy, and stay supersonic to a great distance to push their way through the external medium where a shock front is formed as shown by hot spots. The end of the jets move outwards much more slowly than material flows along the jets. A back flow of relativistic plasma deflected at the end of the jets forms the

lobes. The gaseous environment they inhabit is very important to provide a working surface for the jets to terminate, therefore, the ICM provides an ideal environment for producing FR II radio sources. The observed radio radiation from FR II type radio sources is often highly linearly polarized (e.g. Bonafede et al. 2010). The Laing-Garrington effect strongly suggests the existence of intracluster magneto-ionic material surrounding the radio sources causing asymmetry in the polarization properties of double radio sources with one jet (Laing 1988; Garrington et al. 1988). Many double radio sources have been detected from galaxies at low redshifts ($z < 0.3$), and a large number of sources have been found in dense cluster-like gaseous environments at higher redshifts (Yates et al. 1989; Hill & Lilly 1991; Wan & Daly 1996; Pentericci et al. 2000; Miley & De Breuck 2008).

It is not known if there is any evolution of intracluster magnetic fields at different cosmological epochs. Statistical studies of the redshift evolution of *net* rotation measures contributed by the ICM is the key for the puzzle. Cosmological simulations by Akahori & Ryu (2011) predicted the redshift dependence of extragalactic rotation measures caused by the intergalactic medium. Contributions by galaxy clusters, however, could not be properly modeled given the cell size in their simulations. Previously, there have been a number of works to investigate the redshift evolution of extragalactic rotation measures (Hammond et al. 2012; Neronov et al. 2013; Xu & Han 2014b; Pshirkov et al. 2015; Lamee et al. 2016; O’Sullivan et al. 2017), which were generally made for the whole contributions on the path from the observer to the sources. A marginal dependence of redshift was found. In the early days, the RM differences were also studied for a small number of double radio galaxies at low Galactic latitudes to investigate the enhanced turbulence in the interstellar medium (Simonetti & Cordes 1986; Pedelty et al. 1989; Lazio et al. 1990; Clegg et al. 1992; Minter & Spangler 1996). Athreya et al. (1998) studied 15 radio galaxies at high redshift $z > 2$ with large rotation measures, and claimed their RM contributions are likely to be in the vicinity of the radio sources themselves. Goodlet et al. (2004) and O’Sullivan et al. (2017) concluded that no statistically significant trend was found for the RM difference of two lobes against redshift. Vernstrom et al. (2019) classified a large sample of close pairs and found a significant difference of $\sim 5\text{--}10 \text{ rad m}^{-2}$ between physical pairs (separate components of a multi-component radio galaxy or multiple RMs within one of the components) and random pairs, though the redshift dependence of the physical pairs is not evident. O’Sullivan et al. (2020) used a similar method but high precision RM data from the LOFAR Two-Metre Sky Survey, and they find no significant difference between the ΔRM distributions of the physical and non-physical pairs. In fact, the uncertainty of RM measurement is a very important fac-

tor for the evolution investigation. For example, very small RM differences ($1\text{--}2 \text{ rad m}^{-2}$) between the lobes of large radio galaxies at low redshifts can be ascertained with high precision observations (O’Sullivan et al. 2019; Banfield et al. 2019; Stuardi et al. 2020). RM differences for a larger sample of pure double radio sources is necessary to further investigate their correlation with redshift.

A real pair of two physically associated lobes shown as double radio sources have a small separation and an almost the same flux density, which can be found in the Jansky Very Large Array (JVLA) Sky Survey (NVSS; Condon et al. 1998). Taylor et al. (2009) have reprocessed the 2-band polarization data of the NVSS, and obtained the two-band RMs for 37,543 sources. Xu & Han (2014a) compiled a catalog of reliable RMs for 4553 extragalactic point radio sources. In addition to the previously cataloged RMs, many new RM data are published in the literature. In this paper, we have classified RM pairs in the NVSS RM data and the compiled catalog and later literature since 2014, and cross-identified available galaxy redshift data to obtain RMs and redshifts for 627 pairs. We use these data to study the redshift evolution of RM differences. We introduce the rotation measure data in Section 2 and study the distributions of RM differences of pairs in Section 3. Finally, we discuss our results and present conclusions in Section 4 and Section 5, respectively.

Throughout this paper, a standard ΛCDM cosmology is used, taking $H_0 = 100h \text{ km s}^{-1}\text{Mpc}^{-1}$, where $h = 0.7$, $\Omega_m = 0.3$ and $\Omega_\Lambda = 0.7$.

2. ROTATION MEASURE DATA OF PAIRS

We obtain the RM data for a sample of pairs from the NVSS RM catalog (Taylor et al. 2009) and literature (Xu & Han 2014a, and afterwards). We search for real pairs for the two RM datasets separately, since observation frequencies and resolutions for RM measurements are very different. The NVSS radio images are visual inspected to ensure physical pairs.

2.1. The NVSS RM pairs

In the NVSS RM catalog, RM data and flux density measurements are available for 37,543 “sources”. Here a “source” is an independent radio emission component, while a galaxy can produce a few radio components, e.g. two unresolved lobes in addition to a compact core of a radio galaxy. We cross-matched the catalog against itself, and found 1513 source pairs with a flux density ratio $S_{\text{large}}/S_{\text{small}}$ less than 1.5 and an angular separation between $10''$ and $45''$ (i.e. the angular resolution of the NVSS survey). Flux densities of real pairs from two lobes of radio galaxies are most likely to be consistent with each other because of a similar radio power ejected from the same central black hole. The ratio limit is therefore used to largely excludes false pairs from two

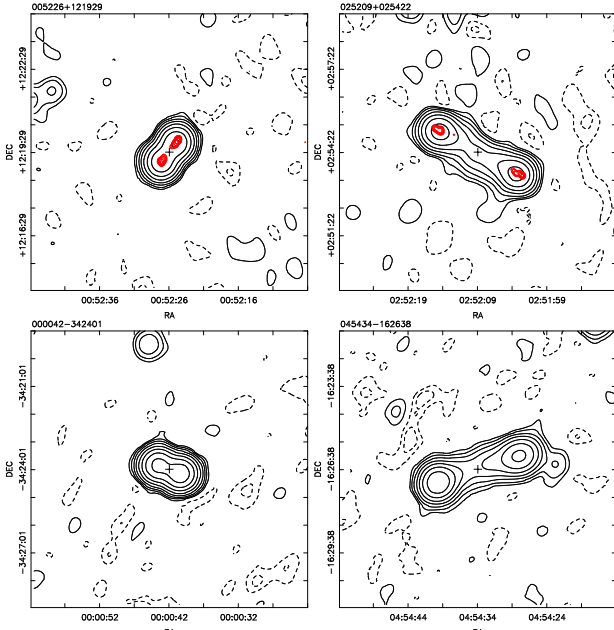


Figure 2. Example images of paired sources from radio galaxies with available RMs in the NVSS RM catalog. The top left is the pair of J005226+121929 ($\Delta r \simeq 0'.89$); the top right is the pair of J025209+025422 ($\Delta r \simeq 3'.05$); the bottom left is the pair of J000042-342401 ($\Delta r \simeq 0'.88$); and the bottom right is the pair of J045434-162638 ($\Delta r \simeq 3'.05$). The pair names here are corresponding to the mean RA and Dec of the pair. The top two pairs are located in the FIRST survey area and therefore the FIRST contours are shown in red. All contours are plotted at levels at $\pm 1, 2, 4, \dots$ mJy beam $^{-1}$, with the plus “+” indicating the central coordinate of double radio sources.

physically unrelated sources. The maximum separation of $10'$ is set for two reasons. The first is that it would be difficult to identify physically related double sources at a larger separation without a clear connection such as diffuse emission between two sources. Second, the number of physical pairs at larger separations is small. In the sample of Vernstrom et al. (2019), only a few pairs have angular sizes greater than $10'$. The minimum separation was set as being the beam size $45''$ of the NVSS survey, so that two very close sources can be just resolved. Vernstrom et al. (2019) adopted two times the beam size, i.e. $1'.5$, while we found the number of physical pairs with separation $\Delta r < 1'.5$ is more than the twice for pairs with $\Delta r > 1'.5$, which is important to get pairs for high redshift galaxies.

Visual inspection was carried out to identify real physical pairs. We obtain the NVSS image centered on the mean RA and Dec of each pair, and make a contour map, as shown in Figure 2. For candidates with angular separations $\Delta r > 3'$, the clear presence of fainter emission connecting the two “sources” is the signature for a real pair, so we get 34 real pairs with $\Delta r > 3'$. For pairs with a smaller angular separation, we check candidates in the survey coverage area

of the VLA Faint Images of the Radio Sky at Twenty centimeters (FIRST; Becker et al. 1995) to verify the true pair. With the experience of classification of real pairs from the NVSS contour maps in the FIRST area, we extrapolate the method to the sources outside the survey area of the FIRST. We noticed that physically unrelated pairs are very scarce at much smaller angular separations (Vernstrom et al. 2019; O’Sullivan et al. 2020). We get 1007 real pairs from the NVSS sources in total. Four examples of identified real pairs are shown in Figure 2.

For these 1007 pairs, we search for their redshifts of the host galaxies from several large optical redshift surveys and online database. First, we cross-match the mean coordinates of RM pairs with the released spectroscopic redshift of 2.8 million galaxies from Data Release 16 of the Sloan Digital Sky Survey (SDSS DR16, Ahumada et al. 2020), and we obtain spectroscopic redshift data for galaxies within 10 arcsec of the given position for 100 pairs. Second, we get another spectroscopic redshifts from the cross-identification of galaxies in the 6dF Galaxy Survey Redshift Catalogue Data Release 3 (Jones et al. 2009) for 10 pairs. We get photometric redshifts for 227 pairs from the cross-match with the SDSS DR8. For the left sources, we cross-identified with the NASA/IPAC Extragalactic Database (NED), and we get redshifts for 64 pairs. In total, we get redshifts and RMs for 401 pairs, as listed in Table A2. The reliability of such cross-match is about 80%, as discussed in the Appendix A. This is the largest sample of RMs for pairs with redshifts currently available for the NVSS RM data.

2.2. The compiled RM pairs

In the compiled RM catalog (Xu & Han 2014a) and more recently published literature after then, RMs are available for many pairs, as listed or presented with radio images in the original references. We inspected all literature and find 444 double sources as real physical pairs. Among them 95 pairs have redshifts already listed in the references or from the NED. For the remaining 349 double sources without redshifts and known host galaxies, we adopted the same procedure for redshift search as for the NVSS RM pairs. The central coordinates of each pair are cross-matched with the SDSS DR16, and we find spectroscopic redshifts for 40 pairs within 10 arcsec. No objects can get the spectroscopic redshift from the 6dF Galaxy Survey data. From the catalog of SDSS DR8, we obtain photometric redshifts for 83 pairs. For the left, we found 8 redshifts from the NED. In total, we have 226 physical pairs with both RMs and redshifts, as listed in Table A1. The redshifts for 95 pairs are very reliable, as marked with ‘*’ in the 10th column, but for the rest 131 pairs, redshift reliability is about 80%. Notice that the redshifts of pairs of $z > 0.9$ are very reliable, because 34 of the 37 pairs have redshifts well measured.

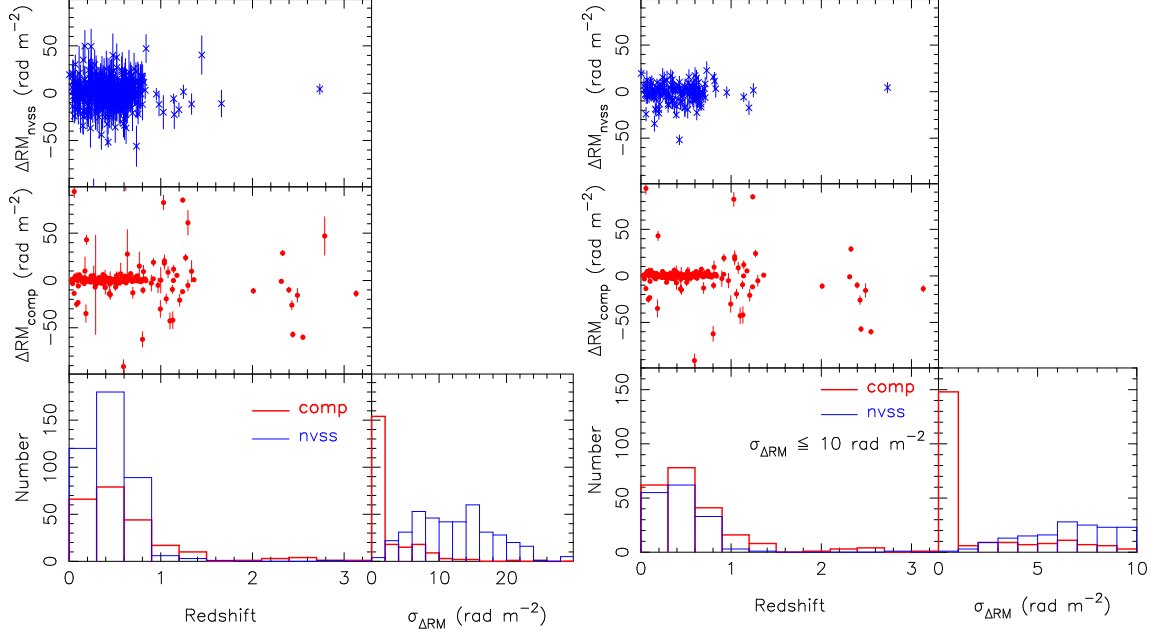


Figure 3. In the left panel, the RM differences ΔRM for 401 pairs from the NVSS data (*top-subpanel*) and for 226 pairs from the compiled data (*middle-subpanel*) and their histograms (*bottom subpanel*) against redshift are shown together with the histograms for uncertainties $\sigma_{\Delta\text{RM}}$. There are 2 and 9 pairs with the ΔRM values outside the value range of the subpanels for the NVSS and compiled data, respectively. The distributions for same data but $\sigma_{\Delta\text{RM}} \leq 10 \text{ rad m}^{-2}$ are shown in the right panel.

2.3. The RM differences of pairs

For a physical pair, i.e. the two lobes of a radio galaxy shown as double radio sources, their radio waves experience almost the same integration path for the Faraday rotation from their inhabited environment in front of the radio galaxy to us, as shown in Figure 1. The RM difference of a pair indicates mostly the immediate difference of the magnetoionic medium in their local environment on a scale comparable to the projected source separation on the sky plane, i.e. a scale from tens of kpc to a few Mpc, though we do not know the angle between the line of sight and the pair connection in 3D. All pairs of sources collected in this work are unresolved point sources, so that their RMs are produced by almost the same intervening medium between the source and the observer. The RM difference $\Delta\text{RM} = \text{RM}_1 - \text{RM}_2$ with an uncertainty of $\sigma_{\Delta\text{RM}} = \sqrt{\sigma_{\text{RM}_1}^2 + \sigma_{\text{RM}_2}^2}$ therefore is the cleanest measurements of Faraday rotation in the ICM, avoiding any additional uncertainties caused by not-well-measured foreground GRM and by the unknown intergalactic contributions such as from cosmic webs and galaxy halos. These unknown uncertainties caused by the foreground of sources are inherited in all traditional statistics for extragalactic RMs.

The RM difference can be negative or positive as we randomly take one to subtract the other, so that statistically the zero mean is expected for a large samples. For our sample the mean of RM difference is -0.21 and -0.11 rad m^{-2} for the NVSS and compiled RM pairs, respectively, which approximate to zero as expected. The distribution of ΔRM for two samples of pairs are shown in Figure 3. The RMs, their dif-

ferences and redshifts of all these 401 and 226 pairs from the compiled data and the NVSS data are listed in Table A2 and A1, respectively, together with angular separation Δr , projected linear separation LS. Only 12 of 401 pairs (3%) of the NVSS RM sources have redshifts larger than 0.9, compared with 37 of 226 pairs (16%) in the compiled sources. In the compiled RM data, 34 double sources marked with '-' in column 11 and 12 have the coordinates for host galaxies but no coordinates for the two radio lobes, and thus the angular and linear separations are not available.

Because the RM uncertainty is a very important factor for the study of the small RM difference of pairs, and because the formal uncertainty of the NVSS RM measurements are much larger than those for the compiled data, the two samples should be analyzed separately. The RM data with small uncertainties are more valuable to reveal the possible evolution with redshift, the subsamples with $\sigma_{\Delta\text{RM}} \leq 10 \text{ rad m}^{-2}$ are taken seriously here and their distribution is shown in the right panel of Figure 3.

3. LARGE RM DIFFERENCE AT HIGH REDSHIFTS

Based on this largest samples of pairs with both RMs and redshift data available so far, we study their evolution with redshift, and check if the RM difference is related to the separations of two sources.

Figure 4 shows the distribution of absolute values of $|\Delta\text{RM}|$ of pairs against the Galactic latitude. Because the RM differences of double sources at low Galactic latitudes may be contaminated by enhanced turbulence in the interstel-

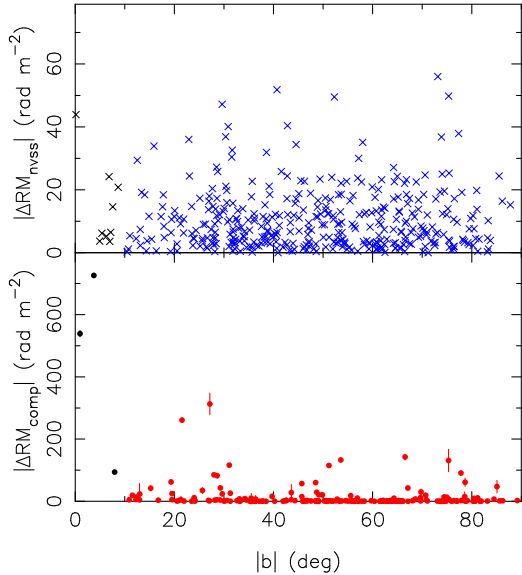


Figure 4. The absolute values of RM difference $|\Delta\text{RM}|$ of pairs from the NVSS data (top panel) and the compiled data (lower panel) against the Galactic latitudes $|b|$. No apparent dependence imply no significant contribution from the ISM. The uncertainties of the NVSS RM data are not shown for clarity.

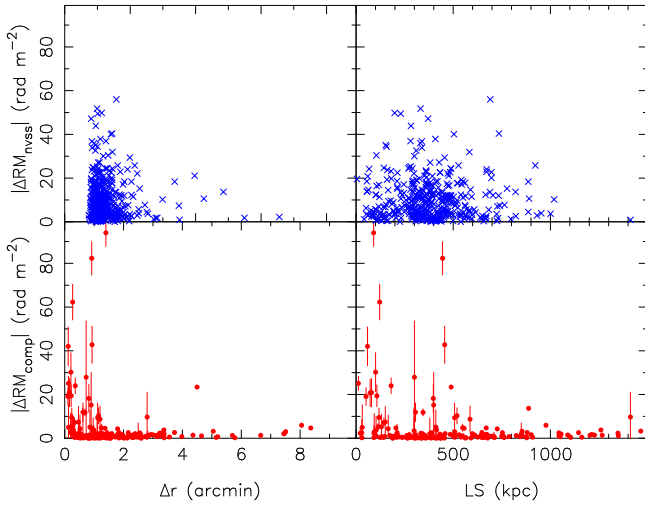


Figure 5. The absolute values of RM difference $|\Delta\text{RM}|$ of pairs for the NVSS data (top panels) and the compiled data (lower panels) against the angular separation (Δr) and the projected linear separation (LS). The uncertainties of the NVSS data are not shown for clarity. A few pairs without the separation values or having a RM difference out of the plotted ranges are not shown.

lar medium when the radio waves pass through the Galactic plane (e.g. Simonetti & Cordes 1986; Clegg et al. 1992; Minter & Spangler 1996), we discard 9 NVSS pairs and 3 pairs from the compiled data at low Galactic latitudes of $|b| < 10^\circ$, though these few pairs may not affect our statistics (see Figure 4). A Spearman rank test demonstrates the absolute $|\Delta\text{RM}|$ of the NVSS data is uncorrelated with Galactic

latitude, with a correlation coefficient of ~ -0.004 (p -value ~ 0.93). For the pairs from the compiled data, only a very weak correlation was found from data, with a correlation coefficient of -0.22 (p -value ~ 0.002). We therefore conclude that the “leakage” to the RM differences from the Galactic interstellar medium can be ignored.

Figure 5 shows the absolute RM difference as a function of the angular separation and projected linear separation of two lobes on the sky plane. For the purpose to explore the magnetic fields in the intracluster medium, we discard 4 pairs with a LS ≥ 1 Mpc from the NVSS data and 25 pairs from the compiled data, because these pairs probably impact much less ICM and their differences may stand more for the RM contribution from the intergalactic medium, given the typical size of galaxy clusters being about 1 Mpc. In addition, one pair from a very distant radio galaxy in the compiled RM data and one pair from the NVSS data have a host galaxy with a redshift of $z > 3$. They are also discarded for the following statistics.

All these discarded pairs are marked with ‘†’ in the column 13 of Table A1 and A2. We finally have a very cleaned 387 NVSS pairs and 197 compiled pairs with a separation of LS < 1 Mpc, $|b| > 10^\circ$ and $z < 3$ for further analysis.

3.1. The RM difference versus redshift

In order to reveal the possible redshift evolution of the small RM difference caused by the intracluster medium, the ΔRM data have to be carefully analyzed.

From Figure 3 and Table A1 and A2, we see that the uncertainties $\sigma_{\Delta\text{RM}}$ from the NVSS RM measurements have a value between 0 and 25 rad m $^{-2}$, and those for the compiled RM data are mostly less than 10 rad m $^{-2}$ and more than half less than 1 rad m $^{-2}$. Xu & Han (2014b) showed that large uncertainties would leak to the ΔRM distribution. Therefore, we have to study the two samples of pairs with very different ΔRM uncertainties separately. We examine two cases, one for the ΔRMs from the whole samples without a threshold of uncertainty, and the other with the threshold of $\sigma_{\Delta\text{RM}} \leq 10$ rad m $^{-2}$.

According to number distribution in Figure 3, we divide the samples of pairs in five redshift ranges, $z=(0.0,0.3)$, $(0.3,0.6)$, $(0.6,0.9)$, $(0.9,1.5)$ and $(2.0,3.0)$, and examine the data dispersion in these ranges as shown in Figure 6, assuming an insignificant evolution of RM differences in a given redshift range. The RM differences of a pair of lobes can be negative or positive, and for an ideal case of a large sample of the ΔRM values should follow a Gaussian distribution with the zero mean. The dispersion, i.e. the width of a Gaussian function $W_{\Delta\text{RM}_{\text{rms}}}$ and can be fitted from the real data distribution of ΔRM , through calculating the root mean square

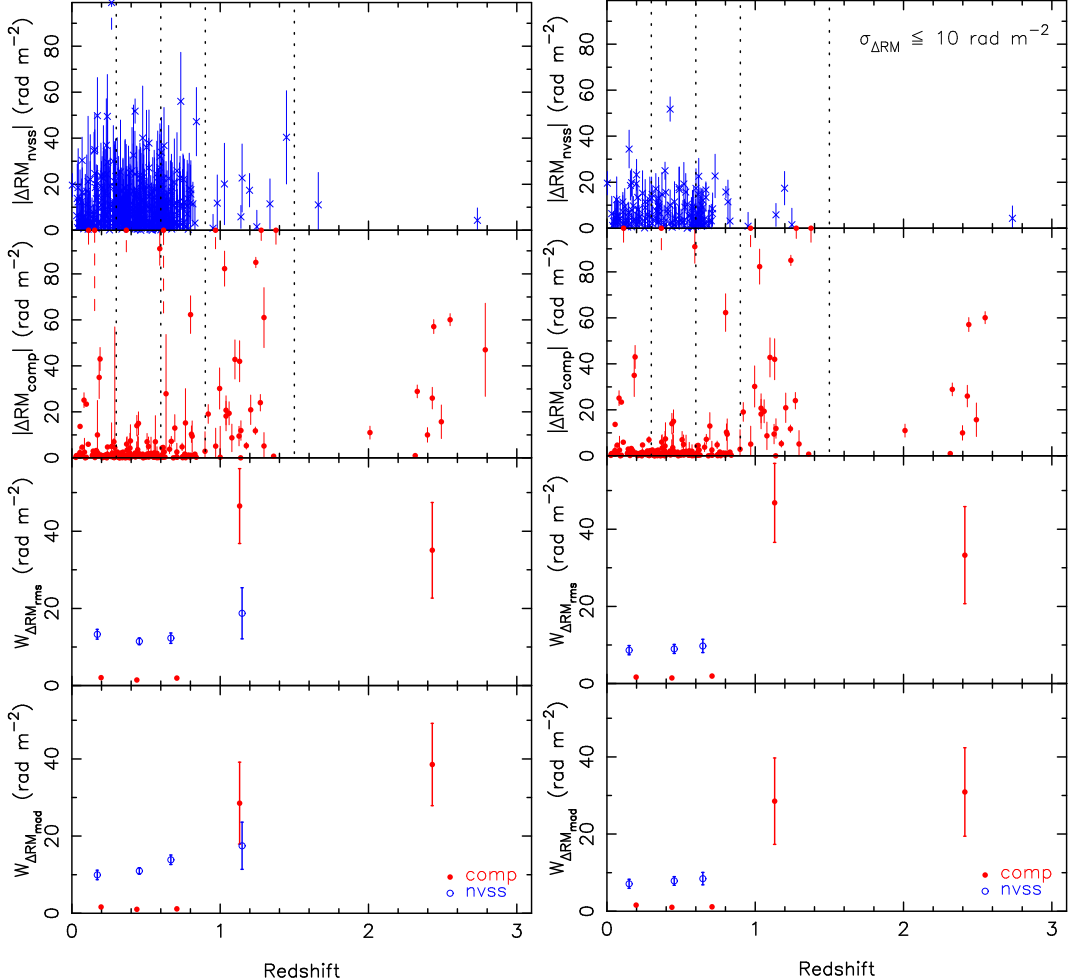


Figure 6. Distribution of absolute values of RM difference $|\Delta\text{RM}|$ and the data dispersions as a function of redshift for 387 NVSS pairs and the 197 pairs of the compiled data with a projected separation of $\text{LS} < 1 \text{ Mpc}$, $|b| > 10^\circ$ and $z < 3$ in the left panel. Sources with $|\Delta\text{RM}| > 100 \text{ rad m}^{-2}$ are plotted at top boundary. The vertical dotted lines in the top two rows indicate the redshift at $z = 0.3, 0.6, 0.9, 1.5$. The dispersions of the ΔRM distribution are calculated with a Gaussian fitting with a characteristic width $W_{\Delta\text{RM}}$, or simply taken as the median absolute values, as shown in the third and fourth rows of panels, respectively. The open circles represent the values from the NVSS RM data, and the filled dots stand for values from the compiled data, plotted at the median redshift for each redshift range. The same plots but for 152 NVSS pairs and 186 compiled pairs with a formal ΔRM uncertainty $\sigma_{\Delta\text{RM}} \leq 10 \text{ rad m}^{-2}$ are shown in the right.

(rms) for the ΔRMs :

$$W_{\Delta\text{RM}_{\text{rms}}} = \sqrt{\frac{\sum_{i=1,N} (RM1 - RM2)_i^2}{N}}, \quad (4)$$

here N is the total number of pairs. Alternatively, a more robust approach is to get the median absolute deviation $W_{\Delta\text{RM}_{\text{mad}}}$, which is good for small data samples and robust in the presence of outliers (cf. Malik et al. 2020). For our ΔRM data, the zero mean is expected. Therefore, we consider the median of the absolute values of the RM difference, i.e.

$$W_{\Delta\text{RM}_{\text{mad}}}^{\text{ori}} = \text{Median}(|RM1 - RM2|_{i=1,N}). \quad (5)$$

For a normally distributed data, this can be linked to $W_{\Delta\text{RM}_{\text{rms}}}$ by $W_{\Delta\text{RM}_{\text{mad}}} = 1.4826 \times W_{\Delta\text{RM}_{\text{mad}}}^{\text{ori}} \simeq W_{\Delta\text{RM}_{\text{rms}}}$ (Leys et al. 2013).

In the redshift ranges with more than five pairs, we calculate the dispersion of RM differences, $W_{\Delta\text{RM}_{\text{rms}}}$ and $W_{\Delta\text{RM}_{\text{mad}}}$, see Table 1 and Figure 6. Though a large ΔRM is possible for embedded double sources contributed from the intracluster medium, with a value maybe up to a few hundred rad m^{-2} (e.g. Clarke et al. 2001), a few outliers are cleaned in our statistics since they affect the calculation of the dispersion of the main stream of data. For the rms calculation, data points scattered away from the main distribution by more than three times the standard deviation are marked as outliers, and removed iteratively until no outliers are marked. The trimmed rms of ΔRM are taken as $W_{\Delta\text{RM}_{\text{rms}}}$ for a subsample in a redshift bin. The uncertainty of $W_{\Delta\text{RM}_{\text{rms}}}$ is taken as the standard error for the zero mean, as done by Vernstrom et al. (2019). For the median calculation, the outliers are also cleaned first, and the median is found from

Table 1. Statistics of the ΔRM distribution for pairs in redshift bins.

Redshift range	No. of pairs	Subsamples from the NVSS RM data			Subsamples from the compiled RM data			
		z_{median}	$W_{\Delta RM_{\text{rms}}}$ (rad m $^{-2}$)	$W_{\Delta RM_{\text{mad}}}$ (rad m $^{-2}$)	$W_{\Delta RM_{\text{mock}}}$ (rad m $^{-2}$)	No. of pairs	z_{median}	$W_{\Delta RM_{\text{rms}}}$ (rad m $^{-2}$)
584 pairs with no uncertainty constraint: 387 NVSS RM pairs and 197 compiled RM pairs								
0.0–0.3	116	0.171	13.3 ± 1.3	9.9 ± 1.2	10.2 ± 3.1	57	0.198	2.1 ± 0.3
0.3–0.6	174	0.455	11.5 ± 0.9	11.0 ± 0.8	10.2 ± 1.6	67	0.439	1.5 ± 0.2
0.6–0.9	86	0.668	12.3 ± 1.3	13.9 ± 1.2	10.7 ± 2.1	39	0.708	2.0 ± 0.4
0.9–1.5	9	1.148	18.7 ± 6.6	17.5 ± 6.1	—	25	1.131	46.5 ± 9.7
2.0–3.0	2	—	—	—	—	9	2.430	35.1 ± 12.4
0.9–3.0	11	1.198	17.3 ± 5.5	17.0 ± 5.1	—	34	1.222	43.7 ± 7.7
338 pairs of $\sigma_{\Delta RM} \leq 10$ rad m $^{-2}$: 152 NVSS RM pairs and 186 compiled RM pairs								
0.0–0.3	54	0.150	8.6 ± 1.2	7.1 ± 1.2	7.4 ± 1.4	53	0.198	1.7 ± 0.3
0.3–0.6	60	0.454	9.0 ± 1.2	7.9 ± 1.1	8.2 ± 0.8	66	0.438	1.5 ± 0.2
0.6–0.9	33	0.647	9.7 ± 1.7	8.5 ± 1.6	8.4 ± 1.9	36	0.709	2.0 ± 0.4
0.9–1.5	4	—	—	—	—	23	1.131	46.8 ± 10.2
2.0–3.0	1	—	—	—	—	8	2.414	33.3 ± 12.6
0.9–3.0	5	—	—	—	—	31	1.201	43.6 ± 8.1

$W_{\Delta RM_{\text{mock}}}$ denotes the “intrinsic” dispersions of the NVSS data derived by the mock method in Appendix B.

the remaining $|\Delta RM|$, which is taken as $W_{\Delta RM_{\text{mad}}}^{\text{ori}}$ and then converted to $W_{\Delta RM_{\text{mad}}}$ with a factor of 1.4826. Its uncertainty is taken as being $\sigma_{\langle |\Delta RM_i| \rangle}$, the error of the estimated mean value of $|\Delta RM|$, also with a factor of 1.4826.

The dispersion calculated above in fact includes a “noise” term coming from various uncertainties of RM values. In principle, the noise term should be discounted from the ΔRM dispersion to get real astrophysical contributions. For each pair, the noise term can be expressed from the quadrature sum of the uncertainty of RMs of two lobes, i.e. for the i th pair, the noise $\sigma_{\Delta RM_i}^2 = (\sigma_{RM1}^2 + \sigma_{RM2}^2)_i$. The procedure of noise subtraction for the dispersion width $\sqrt{W_{\Delta RM_{\text{rms}}}^2 - \langle \sigma_{\Delta RM_i}^2 \rangle}$ should be carried out under the assumption that the uncertainties in the observed RMs provide a realistic estimate of the measurement error. However, RM uncertainties of the NVSS data are underestimated for most sources (Stil et al. 2011) or probably overestimated for physical pairs (Vernstrom et al. 2019), probably caused by a previously unknown systematic uncertainty (Mao et al. 2010; Xu & Han 2014a). For the compiled RM data, different estimation methods were used for measurement errors, or observations with uncorrected ionospheric RM will introduce an extra RM uncertainty about 3 rad m $^{-2}$. It is hard to get a realistic uniformed estimate of the measurement error for the pair sample in this paper. Fortunately for this work the RM difference (ΔRM) 2 is concerned, which can largely diminish any systematical uncertainties which contribute the same amount to the RM measurements of two closely located sources, though a small unknown amount of noise leakage still may occur. We found that the $W_{\Delta RM_{\text{mad}}}$ are even much smaller than the average noise power $\langle \sigma_{\Delta RM}^2 \rangle$, thus no

correction of the noise term is made to dispersion quantities $W_{\Delta RM_{\text{rms}}}$ and $W_{\Delta RM_{\text{mad}}}$ in Table 1.

With these careful considerations above, it is the time to look at the dispersion of RM differences of pairs as a function of redshift z , with or without a threshold of ΔRM uncertainty for the NVSS RM pairs and the compiled RM pairs, respectively. First of all, the amplitudes of dispersion represented by $W_{\Delta RM_{\text{rms}}}$ and $W_{\Delta RM_{\text{mad}}}$ are consistent with each other within error bars, as shown in Table 1 and Figure 6. Second, for the NVSS RM pairs, no significant variation of the dispersion with redshift is seen in both whole sample and the high precision sample with $\sigma_{\Delta RM} \leq 10$ rad m $^{-2}$, which is consistent with the results for physical pairs obtained by Vernstrom et al. (2019). However, the systematically larger dispersion is obtained from the whole sample than that from the high precision sample, which implies the large uncertainty of the NVSS RM values (a noise term around 10.4 rad m $^{-2}$ given by Schnitzeler 2010) significantly affects the dispersion of ΔRM , and probably buries the small amplitude evolution at low redshifts. This is a sign of the some noise leakage which cannot be cleaned. Third, for pairs from the compiled RM data which have very a small noise, a much larger dispersion appears for pairs of $z > 0.9$ in both samples with/without $\sigma_{\Delta RM}$ threshold setting, compared to a small dispersion for pairs of $z < 0.9$. The amplitude of dispersion for pairs of $z < 0.9$ mostly is less than 2 rad m $^{-2}$, but for pairs of $z > 0.9$ the dispersion is about 30 to 40 rad m $^{-2}$. Even the measurement noise, which is about 5.6/4.7 rad m $^{-2}$ at $z > 0.9$ without/with $\sigma_{\Delta RM} \leq 10$ rad m $^{-2}$ threshold is discounted, the result on larger dispersion is not changed. Since the dispersion values

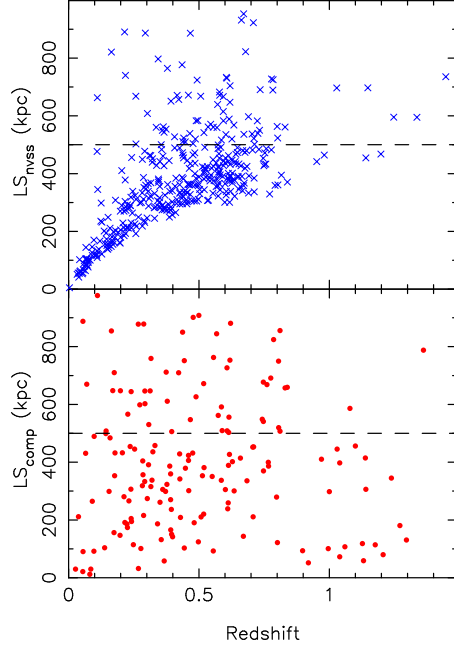


Figure 7. Projected separation of pairs at various redshifts from the NVSS sample (top) and the compiled data (bottom). Note that 34 pairs (14 pairs at $z > 0.9$) in the compiled data are not included since their angular and hence linear separations are not available.

for two redshift ranges of $z > 0.9$ are similar, the data of all pairs in the redshift of $0.9 < z < 3.0$ are therefore jointly analyzed, and the uncertainty becomes smaller. The large dispersion for the high-redshift pairs of $z > 0.9$ is therefore a good detection at about a 5-sigma level.

We note that the pairs with a low redshift in the compiled data are mainly measured at low frequencies by LOFAR (144 MHz) (e.g. O’Sullivan et al. 2020) and MWA (200 MHz) (e.g. Riseley et al. 2020). Low frequency data may probe the outer part of galaxy clusters or poor clusters, hence the dispersion amplitude around 2 rad m^{-2} calculated from pairs of $z < 0.9$ should read as a lower limit of Faraday rotation from the intracluster medium. The dispersion about $7 \sim 9 \text{ rad m}^{-2}$ estimated from the NVSS RM data with $\sigma_{\Delta\text{RM}} \lesssim 10 \text{ rad m}^{-2}$ should be taken as an upper limit. The “intrinsic” dispersions of the NVSS RM data in three low redshift bins at $z < 0.9$ are verified by the mock method introduced by Xu & Han (2014b), see Appendix B.

Based on above results, we conclude that the dispersion of RM differences for pairs of $z < 0.9$ should be a value in the range of $2 \sim 8 \text{ rad m}^{-2}$, much smaller than the value of $30 \sim 40 \text{ rad m}^{-2}$ for high-redshift pairs of $z > 0.9$.

3.2. The RM difference and projected separation

Is the significant change of ΔRM dispersion for pairs at $z > 0.9$ biased by the linear sizes of double radio sources or their separation? Figure 7 shows the projected separation of pairs versus the redshift for both the NVSS and compiled

RM samples. The majority of high-redshift pairs ($z > 0.9$) in the compiled data have a separation less than 500 kpc.

As seen in Figure 5, the absolute values of RM differences decline to small values when a projected separation is larger than 1 Mpc, the typical size of a galaxy cluster. The pairs with such a projected separation greater than 1 Mpc probably lie at a large angle to the line of sight, and their light paths pass through much less content of the intracluster medium.

To examine if the larger RM dispersion of high redshift pairs is caused by different separation, in the following we split the NVSS sample and compiled data sample into two cases, i.e. the subsamples with a separation larger or smaller than 500 kpc. In the compiled sample, 34 pairs (14 sources of $z > 0.9$) are omitted since the angular and hence the linear separations are not available though they are probably smaller than 1 Mpc. Statistics results are shown in Figure 8 and listed in Table 2. No obvious difference of the ΔRM dispersion can be seen between two subsamples with a separation smaller and larger than 500 kpc in all three low redshift bins for both the NVSS data and the compiled data. The dispersion values of subsamples are consistent with the results derived from the whole sample, which means that the redshift-dependent dispersion is not caused by different sizes of pair separation. For high-redshift pairs of $z > 0.9$, statistics can be made for the NVSS subsample with a larger separation than 500 kpc and also the compiled subsample data with a smaller separation. They both show a larger dispersion though with different uncertainties. The larger RM difference is detected at a 4σ level for the compiled subsample.

4. DISCUSSION

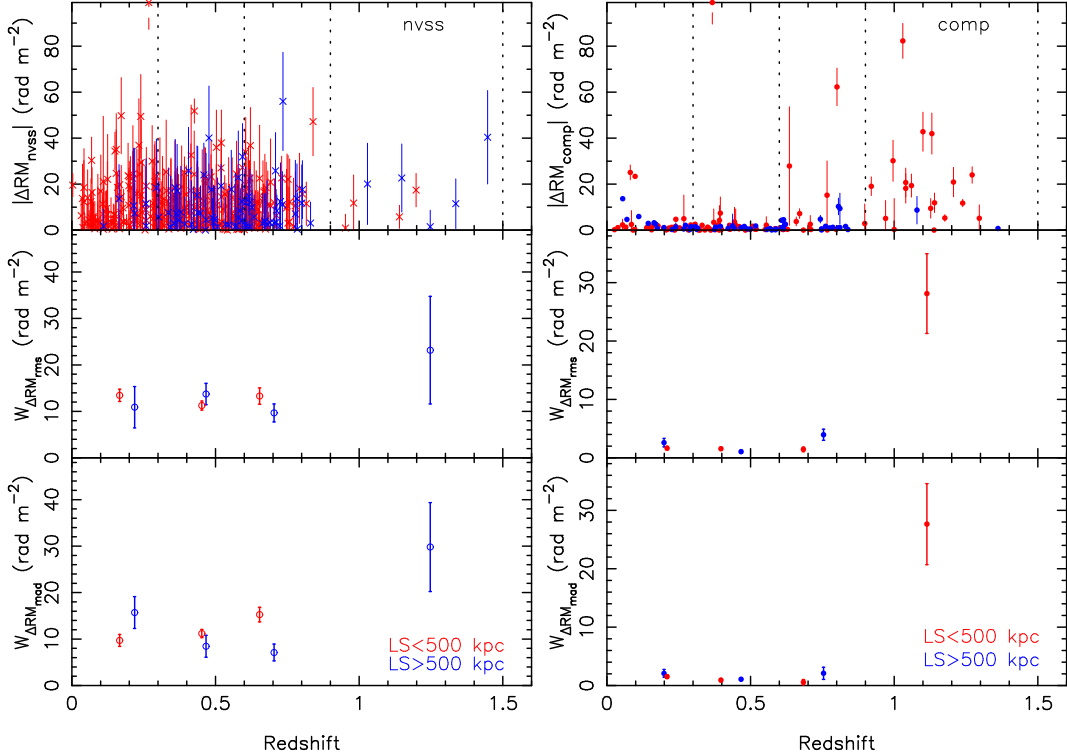
If the larger RM differences of high-redshift pairs were caused by intergalactic medium between the pair and us, the larger the separation between a pair of two lobes, the more likely their radio waves experience different foreground cosmic filaments and intervening medium along the lines of sight. That is to say, the larger the separation of lobe positions, the more likelihood for the larger RM difference (e.g. O’Sullivan et al. 2019). However, for the compiled RM samples in Figure 5 and Figure 8, this is not the case, and the results are just the opposite, which means that the main RM differences are caused by the local ICM environment surrounding the double radio sources, instead of the intervening intergalactic medium in the foreground of a pair of two lobes. Therefore the RM differences of pairs are excellent probes for the ICM.

4.1. Strong magnetic fields in the intracluster medium in the early Universe

Evidence for larger RM differences for higher-redshift pairs, having wisely excluded any obvious influence by the Galactic and intergalactic contributions and also possible dependence on linear separations of pairs, demonstrates the

Table 2. Statistics of the ΔRM distribution for pairs with a separation larger or smaller than 500 kpc.

Redshift range	Subsamples from the NVSS RM data				Subsamples from the compiled RM data			
	No. of pairs	z_{median}	$W_{\Delta RM_{\text{rms}}}$ (rad m $^{-2}$)	$W_{\Delta RM_{\text{mad}}}$ (rad m $^{-2}$)	No. of pairs	z_{median}	$W_{\Delta RM_{\text{rms}}}$ (rad m $^{-2}$)	$W_{\Delta RM_{\text{mad}}}$ (rad m $^{-2}$)
pairs with a separation larger than 500 kpc: 76 NVSS pairs and 54 compiled pairs								
0.0–0.3	7	0.218	10.9 ± 4.5	15.7 ± 3.4	15	0.199	2.6 ± 0.7	2.1 ± 0.7
0.3–0.6	37	0.467	13.7 ± 2.3	8.5 ± 2.4	19	0.467	1.1 ± 0.2	1.1 ± 0.2
0.6–0.9	27	0.704	9.7 ± 1.9	7.1 ± 1.8	18	0.754	4.0 ± 1.0	2.1 ± 1.0
0.9–1.5	5	1.247	23.2 ± 11.6	29.8 ± 9.6	2	—	—	—
pairs with a separation smaller than 500 kpc: 309 NVSS pairs and 109 compiled pairs								
0.0–0.3	109	0.167	13.4 ± 1.3	9.7 ± 1.3	34	0.210	1.7 ± 0.3	1.5 ± 0.3
0.3–0.6	137	0.453	11.3 ± 1.0	11.2 ± 0.9	38	0.397	1.6 ± 0.3	0.9 ± 0.3
0.6–0.9	59	0.653	13.3 ± 1.8	15.3 ± 1.6	19	0.684	1.4 ± 0.4	0.6 ± 0.4
0.9–1.5	4	—	—	—	18	1.114	28.1 ± 6.8	27.7 ± 6.9

**Figure 8.** Absolute RM difference ($|\Delta RM|$) distributions and their dispersion ($W_{\Delta RM_{\text{rms}}}$ and $W_{\Delta RM_{\text{mad}}}$) against redshift for pairs with a separation larger and smaller than 500 kpc for the NVSS RM sample (left) and the compiled data sample (right).

strong magnetic fields in the ICM in the early Universe. We can estimate the field strengths in the ICM from the dispersion of RM differences at the present epoch and at high redshift.

As mentioned in Section 1, a pair of lobes are believed to mainly reside in dense environments of galaxy clusters/groups. Such dense ambient gas plays a key role in forming Faraday screens which contributes to the difference between the RM values of the lobes. The RM asymmetry of a pair of lobes indicates that there probably exists a large-scale

ordered net magnetic fields in the foreground ICM with a scale of pair separation. Because of turbulent nature for intracluster magnetic fields, large scale fluctuations (> 100 kpc) should be responsible for the RM differences of pairs, and a very large outer scale for turbulent intracluster magnetic fields of ~ 450 kpc is possible as being used for modeling of magnetic fields for a giant radio halo (Vacca et al. 2010). The small-scale field fluctuations at a few kpc could be averaged out over a path length comparable to the projected separation.

A pair of radio sources in our sample could have any separation and arbitrary orientations in space. The path difference along the line of sight of the two lobes may vary from zero to the largest linear size. Assuming a unidirectional large-scale magnetic field geometry and a constant electron density in the ambient environs, we get a RM difference as being

$$\Delta RM = 812 n_e B L_{||} \cos \theta, \quad (6)$$

where $L_{||}$ is the separation of the pair (in kpc) projected onto the line of sight, and θ is the angle between the magnetic field direction and the line of sight. For a sample of pairs with the same separation but random directions of magnetic fields, the mean of ΔRM is

$$\langle \Delta RM \rangle = 812 n_e B L_{||} \int_0^\pi \cos \theta \sin \theta d\theta / \int_0^\pi \sin \theta d\theta = 0, \quad (7)$$

and the variance is given by

$$\begin{aligned} \langle (\Delta RM)^2 \rangle &= (812 n_e B L_{||})^2 \int_0^\pi \cos^2 \theta \sin \theta d\theta / \int_0^\pi \sin \theta d\theta \\ &= \frac{1}{3} (812 n_e B L_{||})^2. \end{aligned} \quad (8)$$

Further more, we consider a pair of sources with a random separation L along a random orientation ϕ , i.e. $L_{||} = L \cos \phi$, where L is the size and ϕ is the angle between the orientation and the line of sight. Hence, we expect

$$\begin{aligned} \langle (\Delta RM)^2 \rangle &= \frac{1}{3} (812 n_e B)^2 \langle L^2 \rangle \langle \cos^2 \phi \rangle \\ &= \frac{1}{9} (812 n_e B)^2 \langle L^2 \rangle. \end{aligned} \quad (9)$$

Here $\langle L^2 \rangle$ denotes the mean square of the separation of pairs.

The rest-frame RM dispersion of a Faraday screen at redshift z is expected to be decreased to the observed values by the factor of $(1+z)^2$. Then we can derive an analytical formulation by assuming the field strength and the electron density to be constant in the environs around the double radio sources at redshift z , i.e.

$$\langle (\Delta RM)^2 \rangle = \frac{1}{9} 812^2 \langle L(z)^2 \rangle \left[\frac{n_e(z) B(z)}{(1+z)^2} \right]^2. \quad (10)$$

and finally we get

$$\begin{aligned} W_{\Delta RM_{rms}} &= \langle (\Delta RM)^2 \rangle^{1/2} \\ &= 271 n_e(z) B(z) \langle L(z)^2 \rangle^{1/2} (1+z)^{-2}. \end{aligned} \quad (11)$$

From the Equation (11), we can derive the magnetic fields in the ICM if the dispersion of RM difference, electron density n_e and the variance of the pair separations $\langle L^2 \rangle^{1/2}$ at redshift z are known.

Based on the results shown in Figure 6, the dispersion of the RM difference of pairs remains nearly flat at $z < 0.9$, with an amplitude about 2 to 8 rad m⁻². We take a typical value being 3.5 rad m⁻² to represent the dispersion at the present time. For pairs of $z > 0.9$, the dispersion increases to 30 to 40 rad m⁻² at a median redshift of $z = 1.1$. We take a typical value being 35 rad m⁻² at $z = 1.1$. For the variance of the pair separations $\langle L^2 \rangle^{1/2}$ at redshift z , we take the same typical value of 350 kpc for pairs at low and high redshifts¹. At low redshifts, the mean electron density n_e in the ICM is taken to be 4×10^{-4} cm⁻³, which is obtained by integrating the β -model profile of electron density over a sphere with a radius of 1 Mpc for 12 galaxy clusters (Govoni et al. 2010). According to the Equation (11), from $W_{\Delta RM_{rms}} = 3.5$ rad m⁻², $n_e = 4 \times 10^{-4}$ cm⁻³ and $\langle L^2 \rangle^{1/2} = 350$ kpc at $z = 0$, we can obtain a simple estimation of the magnetic field strength over this scale as being $B = 0.1 \mu G$ at present epoch. At high redshift $z > 0.9$, we do not know the exact properties of the ICM. If we assume the mean electron density $n_e(z)$ at $z > 0.9$ is as same as the density at the present epoch, along with $W_{\Delta RM_{rms}} = 35$ rad m⁻², and $\langle L^2 \rangle^{1/2} = 350$ kpc as well at $z = 1.1$, the magnetic field would be $B(z) = 4 \mu G$. To get this value, any field reversals smaller than 350 kpc are ignored. If the fields reverse at a scale of 30 kpc are considered, the field strength would be boosted by a factor of $\sqrt{350/30}$, reaching the field strength of 14 μG .

4.2. Implication of strong magnetic fields in the ICM

The field strength estimated above for the ICM from the pairs at $z < 0.9$, if in the form of a uniform large-scale field geometry, is $0.1 \mu G$, close to the minimum intracluster magnetic field obtained by Pratley et al. (2013). More tangled fields would have a strength of a few times stronger. The estimated field strength is smaller than that of some targeted clusters, such as a few μG on scales of tens of kpc in merging clusters and a few $10 \mu G$ in cool core clusters (see e.g. Carilli & Taylor 2002; van Weeren et al. 2019). There are two possible reasons. The first one, the well-measured RM differences at low redshifts are predominantly by the RM data with very small uncertainties, which were mainly measured at low frequencies by LOFAR (e.g. O'Sullivan et al. 2020) and MWA (e.g. Risseley et al. 2020). Those observations at such low frequencies may probe medium in the outer part of galaxy clusters or poor clusters, so that the estimated

¹ The average projected linear separation is 281 kpc and 234 kpc for samples of $z < 0.9$ and $z > 0.9$ with a separation smaller than 500 kpc, based on the fact that majority of pairs at $z > 0.9$ have small separations and their dispersions are consistent with those from the whole sample. Considering random projection effect, we estimate the real pair separations should be larger by a factor of $\sqrt{2}=1.4$, i.e. 396 kpc or 329 kpc, respectively.

field strength is close to the large-scale intergalactic magnetic fields around galaxy clusters, as illuminated by simulations (Ryu et al. 2008). In contrast, the small number of RM data with larger uncertainties and more scattered in the distribution were mostly observed at 1.4 GHz or higher frequencies, which are more likely to probe the inner part of galaxy clusters. Secondly, at low redshifts most powerful radio sources reside in comparatively sparse environment with few exceptions [e.g. Cygnus A (Dreher et al. 1987) and other sources of large RM differences in the compiled data], as pointed by Pentericci et al. (2000), so that the dispersion of RM difference is small. This is supported by the NVSS sample with a similar small dispersion of RM difference, i.e. upper limit of 7–9 rad m⁻² derived by this work and 4.6±1.1 rad m⁻² by Vernstrom et al. (2019).

The value of uniform intracluster magnetic field strength of 4 μG (or ∼14 μG for tangled fields) at $z > 0.9$ derived from the RM difference of pairs is intriguing, as it is comparable to the field strength of galaxy clusters at low redshifts (see a review by Han 2017), for example a central field strength of 4.7 μG in the Coma cluster (Bonafede et al. 2010) and a few microGauss in a sample of X-ray selected clusters (Clarke et al. 2001; Böhringer et al. 2016). This is evidence for strong organized magnetic fields in galaxy clusters in the early Universe. If this scenario is correct, it poses a considerable challenge to theories on the origin of intracluster magnetic fields, because time available at $z > 0.9$ is not sufficient to generate and align strong magnetic fields on such a large scales. The building-up of large-scale coherent magnetic fields via the inverse cascade of the $\alpha-\Omega$ dynamo fields that often works in normal spiral galaxies cannot operate in galaxy clusters because they do not have an observed organized rotation. Even if they have, only one or two rotations at this age of the Universe under slow cluster rotation ($v \leq 100$ km s⁻¹) is insufficient for generation of such a strong mean field (Carilli & Taylor 2002).

The origin and the growth of magnetic fields in galaxy clusters are an enigma. The widely accepted hypothesis is that they are amplified from much weaker seed fields (either primordial or injected by galactic outflows) through a variety of processes (see review Donnert et al. 2018). Simulations show evidence of significant magnetic field amplification with a small-scale dynamo driven by turbulence and

compression during structure formation (Vazza et al. 2018; Domínguez-Fernández et al. 2019). Assuming the dynamo growth can start soon after the cluster forms, it often takes a time-span of several Gyr to amplify magnetic fields to a few μG (e.g. Domínguez-Fernández et al. 2019). Increasing the Reynolds number can reduce the time scale for magnetic amplification, but the number is limited by the efficiency of the transfer of kinetic energy into magnetic energy. Merger induced shocks that sweep through the ICM or motions induced by sloshing cool cores may play additional roles in fast amplification of intracluster magnetic field at high redshifts (Donnert et al. 2018), but not up to such a large scale. The recent observations of diffuse radio emission in distant galaxy clusters (Di Gennaro et al. 2021) have put a strong limit on the time scale of the magnetic growth by discovering field strengths of μG at $z \sim 0.7$. The time available for the amplification in their case is about 3.7 Gyr. Our results is strong evidence for strong magnetic field strengths at such a large-scale at $z > 0.9$ and even up to $z \sim 2$, comparable to those in nearby clusters, which is a more stringent constraint for magnetic field generation and evolution.

5. CONCLUSIONS

Faraday rotation measure differences between the two lobes of a sample of radio galaxies, which is completely free from the Faraday rotation effect contributed from the interstellar medium inside the Milky Way and the intergalactic medium between radio galaxies and us, is significantly large at $z > 0.9$, indicating the average intracluster magnetic fields about 4 μG (or 14 μG for tangled fields), in contrast to the weaker intracluster fields at the present epoch about 0.1 μG (or 0.3 μG for tangled fields). Such a strong magnetic fields in the early universe makes a big challenge on the generation of cosmic magnetic fields.

More RM data for pairs at high redshift are desired to reach firm conclusion, since current data sets are not enough in number and have somehow large measurement uncertainties. Polarization observations for RMs of a larger sample of double radio sources with a better precision of RMs should be available soon, which are necessary to further constrain the evolution of magnetic fields in the ICM.

APPENDIX

A. COMPARISON OF REDSHIFT DATA OF PAIRS WITH THOSE IN VERNSTROM ET AL. (2019)

Vernstrom et al. (2019) obtained 317 physical pairs of polarized sources at Galactic latitudes $|b| \geq 20^\circ$, with a polarization fraction of $\geq 2\%$ and an angular separation between

1'.5 and 20' from the NVSS RM catalog (Taylor et al. 2009). These pairs include not only pairs of lobes, but also separated components of some multi-component radio galaxies or even multiple RMs within one of the components (e.g., two RM measurements within one AGN jet or lobe). Among these 317 pairs, 208 of them have been found to have spectroscopic

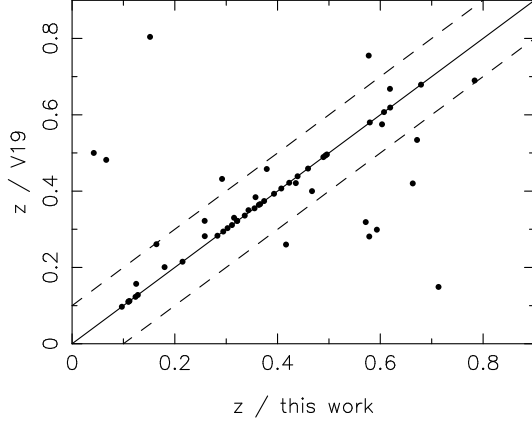


Figure A1. Comparison of redshifts for 56 pairs in Vernstrom et al. (2019), V19 and our sample. The solid line is the equal line, and the dashed lines denote the redshift offset of ± 0.1 .

or photometric redshifts by performing a redshift search from the catalogs of Hammond et al. (2012) and Kimball & Ivezić (2008, 2014) as well as their own compiled ERG catalog of extended radio galaxies.

We get 1007 real pairs, i.e. double-lobed radio galaxies, based on visual inspection of the NVSS images with limits on the flux density ratio S_{\max}/S_{\min} within 1.5 and the angular separation between $10'$ and $45''$. The FIRST images are also used to help classify physical pairs for small angular separations at $\Delta r < 3'$. By crossmatching the mean coordinates of RM source positions with several large optical redshift surveys and online database, we obtained spectroscopic or photometric redshifts for 401 pairs.

Based on a different approach from Vernstrom et al. (2019) to get our RM pairs and various cross-matches for redshift, we obtained the large sample of pairs. Comparing our pairs with those in Vernstrom et al. (2019), we get 56 common samples (see Figure A1), and 44 of them have redshifts consistent with each other in ± 0.1 . The identifications of host galaxies and redshifts in Vernstrom et al. (2019) are probably more reliable because they considered morphological information, rather than a simply cross-matching of the central coordinates of pairs with optical positions as our work. However, our straightforward approach is a preferable method under the current condition to obtain a large sample of double radio sources with redshifts. The reliability of our redshifts, if we take the redshifts of 56 common pairs from Vernstrom et al. (2019) as the standard, should be 44/56, i.e. about 80%.

B. APPLICATION OF MOCK METHOD TO THE REDSHIFT BINS AT $Z < 0.9$ FOR THE NVSS DATA

We tried to use the mock method introduced by Xu & Han (2014b) to derive the intrinsic dispersion of a data sample by carefully discarding the effects from measurement uncer-

tainties. As done in Xu & Han (2014b), we use the bootstrap method to obtain the intrinsic dispersion of RM difference ($\Delta RM = RM_1 - RM_2$) distribution given a variety of uncertainties of $\sigma_{\Delta RM} = \sqrt{\sigma_{RM1}^2 + \sigma_{RM2}^2}$. It is clear that the probability of a ΔRM value follows a Gaussian function centred at the ΔRM value with a width of the uncertainty value, i.e.

$$p(\Delta RM) = \frac{1}{\sqrt{2\pi}\sigma_{\Delta RM_i}} \exp \left[-\frac{(\Delta RM - \Delta RM_i)^2}{2\sigma_{\Delta RM_i}^2} \right], \quad (B1)$$

where $\Delta RM_i = (RM_1 - RM_2)_i$ is the RM difference of the i th of pair in the sample, and $\sigma_{\Delta RM_i}$ is its uncertainty. Then, we sum the probability distribution function (PDF) for all ΔRM of a subsample of pairs in a redshift range,

$$P(\Delta RM) = \sum_1^N p(\Delta RM_i). \quad (B2)$$

This contains the contributions not only from the intrinsic distribution width but also the effect of the ΔRM uncertainties. For an ideal data set without any measurement uncertainty, the PDF follow a Gaussian distribution with the zero mean and a standard deviation of $W_{\Delta RM}$, which is the intrinsic dispersion of ΔRM distribution. Because we make statistics of the absolute difference of two RMs, we obtain the final PDF only in the positive side by summing the two half sides of negative and positive profiles.

Such a method should work well for a larger sample, but does not work well in the case of a small sample number (e.g. $n < 30$) or mostly a very small uncertainty (e.g. $\sigma < 0.1 \text{ rad m}^{-2}$). For the NVSS pairs in three redshift bins at $z < 0.9$, we got good results.

Following the method introduced by Xu & Han (2014b), we generate a mock sample of ΔRM with a sample size 50 times of the original ΔRM data with a ΔRM uncertainty randomly taken from the measured ΔRM s. We then sum the PDF of ΔRM for the mock data as done for the real data. Finally, by comparing the two PDFs, $P(\Delta RM)$ and $P_{\text{mock}}(\Delta RM)$ as shown in Figure B1 and B2, we got the dispersions at $z=(0.0, 0.3)$, $(0.3, 0.6)$, $(0.6, 0.9)$ as being 10.2 ± 3.1 , 10.2 ± 1.6 and 10.7 ± 2.1 for the whole sample, and 7.4 ± 1.4 , 8.2 ± 0.8 and 8.4 ± 1.9 for the sample with $\sigma_{\Delta RM} \leq 10 \text{ rad m}^{-2}$, also listed in Table 1. The decrease of the derived dispersions of the whole sample to that of the sample with $\sigma_{\Delta RM} \leq 10 \text{ rad m}^{-2}$ indicates the leakage of measurement uncertainties to the dispersions. Therefore, we conclude that the dispersions at $z < 0.9$ being $7\text{--}9 \text{ rad m}^{-2}$ from the NVSS sample with $\sigma_{\Delta RM} \leq 10 \text{ rad m}^{-2}$ is the only upper limit of intrinsic dispersion.

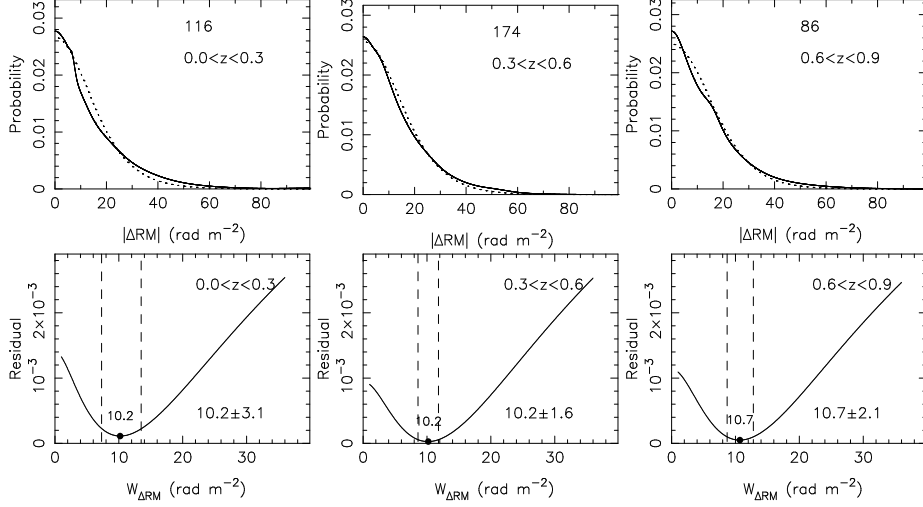


Figure B1. PDF of ΔRM values (solid line), compared with that of the mock ΔRM sample with the best distribution dispersion $W_{\Delta RM}$ (dotted line), for the whole NVSS sample in three redshift bins at $z < 0.9$. The fitting residuals against various dispersion are plotted in the lower panels, which define the best dispersion and its uncertainty at 68 percent probability.

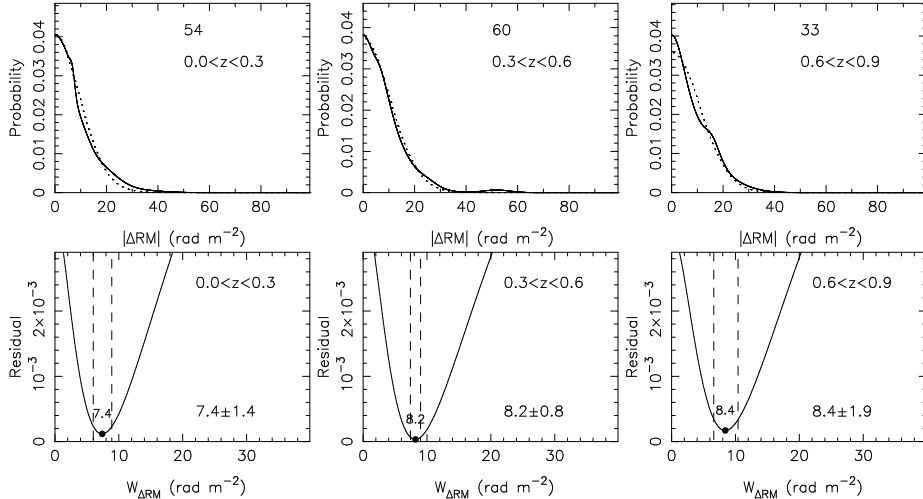


Figure B2. Same as Figure B1 but for the NVSS sample with $\sigma_{\Delta RM} \leq 10 \text{ rad m}^{-2}$.

Table A1. 226 double radio sources with RM and redshift data from the compiled data.

Source 1				Source 2				Ref.	z	Δr	LS	ΔRM	$\sigma_{\Delta RM}$
RA1	Dec1	RM1	σ_{RM1}	RA2	Dec2	RM2	σ_{RM2}						
(deg)	(deg)	(rad m⁻²)		(deg)	(deg)	(rad m⁻²)				(arcmin)	(kpc)		
1.1879	12.8131	-14.504	0.058	1.2429	12.8000	-13.036	0.164	rgs+20	0.1430*	3.31	499	-1.468	0.174
2.6054	33.4822	-41.500	1.300	2.6071	33.5031	-46.300	1.000	sc86	0.7430*	1.25	549	4.800	1.640
3.8079	-35.4469	-2.000	7.000	3.8079	-35.4469	-63.000	11.000	opa+17	1.2960*	—	—	61.000	13.038
4.4926	-22.6344	8.300	2.100	4.4926	-22.6344	19.300	1.900	akm+98	2.0100*	—	—	-11.000	2.832
4.5386	31.0220	-76.848	0.045	4.5350	31.0632	-77.338	0.016	obv+20	0.4996	2.48	908	0.490	0.048
7.2502	29.7044	-62.950	0.010	7.2732	29.7005	-60.584	0.007	obv+20	0.3882	1.22	386	-2.366	0.012

Table A1 continued

Table A1 (*continued*)

Source 1				Source 2				Ref.	z	Δr	LS	ΔRM	$\sigma_{\Delta RM}$
RA1	Dec1	RM1	σ_{RM1}	RA2	Dec2	RM2	σ_{RM2}						
(deg)	(deg)	(rad m $^{-2}$)		(deg)	(deg)	(rad m $^{-2}$)							
9.6121	-38.9961	-62.000	7.000	9.6121	-38.9961	29.000	2.000	opa+17	0.5930*	—	—	-91.000	7.280
10.4137	41.5087	-86.000	9.000	10.4142	41.5109	-91.000	5.000	hbb98	0.2681	0.13	32	5.000	10.296
11.0208	-31.7850	-1.000	7.000	11.0208	-31.7850	-48.000	19.000	opa+17	2.7880*	—	—	47.000	20.248
11.1420	12.1907	-15.581	0.013	11.1510	12.1807	-14.323	0.005	obv+20	0.2258	0.80	249	-1.258	0.014
11.4967	22.4483	-45.683	0.016	11.6320	22.4519	-48.699	0.026	obv+20	0.3282	7.51	2135	3.016†	0.031
15.3475	29.4813	-67.635	0.043	15.3775	29.4648	-70.170	0.028	obv+20	0.6188	1.85	753	2.535	0.051
20.3336	23.8558	-40.969	0.017	20.3008	23.8634	-41.096	0.008	obv+20	0.1554	1.85	299	0.127	0.019
21.2941	27.7461	-55.993	0.029	21.2705	27.7245	-60.289	0.012	obv+20	0.6075	1.80	727	4.296	0.031
21.5336	25.0513	-42.543	0.030	21.5346	25.0938	-45.003	0.023	obv+20	0.6267	2.55	1044	2.460†	0.038
22.1224	29.0530	-2.400	5.000	22.1291	29.0477	5.000	5.000	gkb+04	0.3950*	0.47	150	-7.400	7.071
23.2947	28.7555	-50.488	0.017	23.2847	28.7568	-50.532	0.014	obv+20	0.4816	0.53	190	0.044	0.022
23.4904	-36.4933	2.600	0.300	23.4904	-36.4933	1.700	0.300	bowe19	0.0297*	—	—	0.900	0.424
23.8964	37.9121	-4.800	5.000	23.8476	37.8963	-2.900	1.000	gkb+04	0.4373*	2.50	850	-1.900	5.099
24.4292	15.7097	-38.000	4.000	24.4292	15.7097	-23.000	3.000	hbe09	0.4496	—	—	-15.000	5.000
28.1350	-33.6639	-4.000	1.000	28.1350	-33.6639	-135.000	36.000	opa+17	0.6180*	—	—	131.000	36.014
33.6133	32.8694	-68.567	0.008	33.5217	32.8355	-65.392	0.007	obv+20	0.1643	5.05	855	-3.175	0.011
35.6671	43.0369	-91.900	4.500	35.6658	43.0319	-88.300	4.500	ms96	0.4440*	0.30	103	-3.600	6.364
35.9279	40.0153	-85.400	1.400	35.9329	40.0147	-90.700	0.500	ms96	1.1760*	0.23	114	5.300	1.487
37.9571	39.5519	-103.900	7.600	37.9525	39.5492	-41.600	3.000	ms96	0.8010*	0.27	122	-62.300	8.171
38.1204	34.3906	-70.300	1.600	38.1192	34.4019	-58.500	0.200	ms96	1.2380*	0.69	345	-11.800	1.612
49.5500	-25.5863	0.600	2.400	49.5500	-25.5863	14.500	2.400	akm+98	3.1307*	—	—	-13.900†	3.394
54.7008	-35.3719	26.000	1.000	54.7008	-35.3719	159.000	6.000	opa+17	0.1130*	—	—	-133.000	6.083
55.5229	-37.0561	-3.000	1.000	55.5229	-37.0561	4.000	1.000	opa+17	0.2840*	—	—	-7.000	1.414
57.7995	-20.9665	54.800	1.700	57.7995	-20.9665	25.900	2.200	akm+98	2.3290*	—	—	28.900	2.780
57.8529	-27.7689	34.884	0.023	57.9421	-27.7161	33.590	0.014	rgs+20	0.0656*	5.70	431	1.294	0.027
62.2145	-24.3046	17.300	2.600	62.2145	-24.3046	74.400	1.600	akm+98	2.4400*	—	—	-57.100	3.053
76.4100	-28.9311	15.357	0.033	76.4442	-28.3950	18.615	0.056	rgs+20	0.0382*	32.22	1465	-3.258†	0.065
93.0171	-40.0350	14.846	0.072	93.0921	-39.9831	15.927	0.133	rgs+20	0.0382*	4.65	211	-1.081	0.151
99.1321	-20.4789	36.624	0.028	99.1408	-20.7089	50.286	0.017	rgs+20	0.0551*	13.81	888	-13.662	0.033
107.2608	-35.9819	62.450	0.039	107.4008	-36.0539	56.514	0.022	rgs+20	0.1110*	8.05	977	5.936	0.045
108.5206	14.6064	93.600	1.300	108.5187	14.6058	74.500	3.900	prm+89	0.9200*	0.11	52	19.100	4.111
114.2623	28.8337	2.907	0.029	114.2235	28.8206	2.184	0.017	obv+20	0.4441	2.19	752	0.723	0.034
120.5979	-9.9561	-32.985	0.083	120.7371	-9.9811	-37.678	0.122	rgs+20	0.0699*	8.36	670	4.693	0.148
125.3767	34.6483	15.278	0.067	125.3510	34.6320	17.418	0.041	obv+20	0.3315	1.60	458	-2.140	0.079
128.0838	38.3543	25.425	0.054	128.0856	38.3355	25.370	0.033	obv+20	0.3914	1.13	360	0.055	0.063
128.7593	14.1986	-13.000	4.000	128.7679	14.1961	-17.300	5.000	gkb+04	0.3920*	0.52	166	4.300	6.403
129.4656	44.8219	5.962	0.016	129.4736	44.8570	6.053	0.005	obv+20	0.2065	2.13	433	-0.091	0.017
129.9728	29.4665	19.451	0.013	129.9584	29.4728	19.460	0.010	obv+20	1.1384	0.84	415	-0.009	0.016
130.2956	44.8461	6.605	0.013	130.2709	44.8473	6.306	0.008	obv+20	0.7097	1.05	453	0.299	0.015
136.9504	51.1069	-13.867	0.054	136.9662	51.1096	-13.454	0.025	obv+20	0.4294	0.62	209	-0.413	0.060
137.2124	37.8050	5.900	6.600	137.2083	37.8059	8.800	5.300	prm+89	0.8975*	0.20	93	-2.900	8.465
138.1298	51.4294	-14.304	0.028	138.1645	51.3958	-16.402	0.012	obv+20	0.2733	2.39	599	2.098	0.030
141.6220	43.2026	0.955	0.042	141.6554	43.2244	2.338	0.023	obv+20	0.3786	1.96	611	-1.383	0.048
142.0185	35.1695	17.165	0.010	141.9039	35.1921	16.939	0.021	obv+20	0.3240	5.78	1629	0.226†	0.023

Table A1 *continued*

Table A1 (continued)

Source 1				Source 2									
RA1	Dec1	RM1	σ_{RM1}	RA2	Dec2	RM2	σ_{RM2}	Ref.	z	Δr	LS	ΔRM	$\sigma_{\Delta \text{RM}}$
(deg)	(deg)	(rad m $^{-2}$)		(deg)	(deg)	(rad m $^{-2}$)				(arcmin)	(kpc)	(rad m $^{-2}$)	
142.3336	41.8275	7.842	0.011	142.2523	41.7346	6.540	0.022	obv+20	0.3636	6.66	2024	1.302 \dagger	0.025
142.5286	66.2952	-17.694	0.043	142.5017	66.2834	-17.414	0.036	obv+20	0.6132	0.96	389	-0.280	0.056
142.8042	21.4667	4.000	2.000	142.8042	21.4667	2.000	2.000	hbe09	0.5741	—	—	2.000	2.828
144.6084	23.1298	22.585	0.048	144.5758	23.1424	21.018	0.017	obv+20	0.3076	1.95	531	1.567	0.051
145.7593	28.5659	21.475	0.009	145.7603	28.5897	21.389	0.006	obv+20	0.5739	1.43	562	0.086	0.011
146.1090	43.5696	7.799	0.006	146.1035	43.5459	8.097	0.009	obv+20	0.8390	1.44	659	-0.298	0.011
146.5755	39.7388	1.600	2.000	146.5787	39.7383	-19.100	6.000	gkb+04	1.0400*	0.15	73	20.700	6.325
147.9651	56.1216	5.249	0.056	147.9040	56.1101	7.819	0.040	obv+20	0.6214	2.16	881	-2.570	0.069
148.7203	40.9653	6.242	0.028	148.7412	41.0042	7.873	0.024	obv+20	0.4780	2.52	901	-1.631	0.037
149.4335	51.4754	5.229	0.026	149.3916	51.5225	2.890	0.024	obv+20	0.6545	3.23	1348	2.339 \dagger	0.035
149.5340	53.8325	7.875	0.029	149.5176	53.8428	8.561	0.019	obv+20	0.5857	0.85	337	-0.686	0.035
151.2279	35.0261	3.230	0.020	151.9179	34.6869	9.071	0.006	sob+20	0.1005*	39.60	4404	-5.841 \dagger	0.021
151.4465	21.2708	8.140	0.062	151.4736	21.2917	8.439	0.046	obv+20	0.5562	1.97	762	-0.299	0.077
152.6801	43.9031	5.820	0.006	152.7235	43.9030	6.826	0.007	obv+20	0.2532	1.88	445	-1.006	0.009
153.5553	36.2944	30.800	5.000	153.5483	36.2819	12.600	4.000	gkb+04	1.0400*	0.82	398	18.200	6.403
154.2583	52.3972	4.093	0.058	154.2423	52.3871	3.373	0.040	obv+20	0.2416	0.85	195	0.720	0.070
155.2153	48.5578	5.148	0.005	155.2317	48.4728	5.535	0.005	obv+20	0.2216	5.15	1104	-0.387 \dagger	0.007
155.3158	37.2488	0.900	3.000	155.3038	37.2322	11.200	2.000	gkb+04	0.8060*	1.15	520	-10.300	3.606
156.7500	41.6501	4.797	0.034	156.7466	41.6626	4.022	0.030	obv+20	0.6013	0.76	305	0.775	0.045
156.8893	48.2781	5.495	0.048	156.8882	48.2981	4.917	0.037	obv+20	0.2314	1.20	266	0.578	0.061
160.1416	55.1639	2.546	0.035	160.1635	55.1714	2.638	0.033	obv+20	0.7668	0.87	386	-0.092	0.048
161.6731	54.5744	8.380	0.004	161.5931	54.6304	6.960	0.004	obv+20	0.3233	4.36	1227	1.420 \dagger	0.006
162.5755	79.5603	-28.546	0.028	162.6670	79.5406	-27.553	0.027	obv+20	0.7757	1.55	691	-0.993	0.039
163.0873	37.4879	11.075	0.046	163.1179	37.5175	11.388	0.018	obv+20	0.3742	2.30	712	-0.313	0.049
164.2571	48.6131	16.940	0.003	164.3392	48.7250	19.010	0.040	sob+20	0.2760*	7.46	1881	-2.070 \dagger	0.040
164.2758	53.4300	12.855	0.002	164.2642	53.4481	12.200	0.010	sob+20	0.4600*	1.16	406	0.655	0.010
164.2790	53.4295	12.683	0.003	164.2665	53.4483	12.019	0.008	obv+20	0.4599	1.21	424	0.664	0.009
164.2802	58.7818	13.380	0.007	164.2432	58.7962	11.790	0.009	obv+20	0.8305	1.44	657	1.590	0.011
164.3405	48.7250	18.827	0.024	164.2605	48.6126	16.766	0.003	obv+20	0.4084	7.45	2434	2.061 \dagger	0.024
165.5079	47.7073	23.587	0.039	165.5348	47.7255	23.482	0.015	obv+20	0.7469	1.54	677	0.105	0.042
165.7038	53.2124	18.476	0.005	165.7295	53.2296	18.737	0.006	obv+20	0.2855	1.38	356	-0.261	0.008
167.1264	-26.0851	12.700	1.900	167.1264	-26.0851	38.700	4.300	akm+98	2.4300*	—	—	-26.000	4.701
167.3629	53.2550	11.180	0.060	167.4221	53.2111	11.390	0.070	sob+20	0.2880*	3.38	879	-0.210	0.092
167.8754	35.6805	15.700	6.000	167.8936	35.6760	58.500	6.000	gkb+04	1.1000*	0.93	456	-42.800	8.485
168.3992	46.3811	4.040	0.060	168.3808	46.3639	4.570	0.090	sob+20	0.5890*	1.28	509	-0.530	0.108
168.6231	34.0510	4.445	0.036	168.5863	34.0253	2.577	0.006	obv+20	0.1782	2.39	432	1.868	0.036
169.8667	13.0472	13.000	1.000	169.8667	13.0472	23.000	3.000	hbe09	2.3979	—	—	-10.000	3.162
170.0723	43.9183	28.800	0.015	170.0620	43.9107	29.152	0.006	obv+20	0.6122	0.64	259	-0.352	0.016
171.5250	50.3908	6.022	0.016	171.5255	50.3696	6.609	0.008	obv+20	0.4261	1.28	429	-0.587	0.018
173.1465	36.9062	-19.300	4.000	173.1496	36.9034	0.100	3.000	gkb+04	1.0600*	0.22	107	-19.400	5.000
174.3787	61.3119	0.783	0.012	174.3123	61.3534	2.156	0.006	obv+20	0.6066	3.14	1267	-1.373 \dagger	0.013
175.1470	47.5611	21.064	0.048	175.1779	47.5492	23.627	0.023	obv+20	0.3069	1.44	391	-2.563	0.053
175.4600	-35.0689	25.000	2.000	175.4600	-35.0689	60.000	9.000	opa+17	0.1840*	—	—	-35.000	9.220
176.3590	31.5651	42.200	6.000	176.3800	31.5599	32.800	3.000	gkb+04	0.8110*	1.12	507	9.400	6.708

Table A1 continued

Table A1 (*continued*)

Source 1				Source 2									
RA1	Dec1	RM1	σ_{RM1}	RA2	Dec2	RM2	σ_{RM2}	Ref.	z	Δr	LS	ΔRM	$\sigma_{\Delta \text{RM}}$
(deg)	(deg)	(rad m ⁻²)		(deg)	(deg)	(rad m ⁻²)			(arcmin)	(kpc)		(rad m ⁻²)	
177.4912	12.7898	-9.600	3.000	177.4809	12.7878	-21.500	3.000	gkb+04	1.1400*	0.62	306	11.900	4.243
178.2567	33.4277	-5.782	0.020	178.2402	33.4238	-6.072	0.010	obv+20	0.0973	0.85	92	0.290	0.022
178.4550	-30.1639	-55.000	1.000	178.4550	-30.1639	61.000	6.000	opa+17	1.3760*	—	—	-116.000	6.083
178.5855	18.7190	-9.106	0.038	178.5959	18.7014	-10.063	0.024	obv+20	0.4762	1.21	432	0.957	0.045
180.1192	73.0121	21.700	5.000	180.0704	73.0127	26.800	6.000	gkb+04	0.9700*	0.86	410	-5.100	7.810
180.3108	49.3839	22.030	0.050	180.3800	49.4581	22.700	0.020	sob+20	0.2050*	5.20	1050	-0.670†	0.054
180.7660	23.8992	4.726	0.029	180.7427	23.8742	3.340	0.016	obv+20	0.1764	1.97	353	1.386	0.033
182.1649	-34.0520	-34.000	2.000	182.1649	-34.0520	-119.000	1.000	bbh+07	1.2400*	—	—	85.000	2.236
183.3715	46.0097	2.533	0.049	183.3750	45.9822	1.551	0.015	obv+20	0.8055	1.66	750	0.982	0.051
184.5417	14.2611	-13.000	3.000	184.5417	14.2611	0.000	5.000	hbe09	0.6946	—	—	-13.000	5.831
184.5742	53.4411	15.300	0.030	184.5692	53.4769	14.570	0.030	sob+20	0.5680*	2.16	845	0.730	0.042
184.6592	50.4311	27.784	0.003	184.7421	50.4450	26.682	0.005	sob+20	0.1990*	3.28	647	1.102	0.006
186.1265	39.5296	-11.106	0.048	186.1325	39.5459	-9.450	0.047	obv+20	0.3021	1.02	274	-1.656	0.067
186.4679	53.1531	13.100	0.080	186.5142	53.1681	11.900	0.040	sob+20	0.8110*	1.89	856	1.200	0.089
186.5152	53.1661	11.715	0.030	186.4695	53.1522	12.945	0.046	obv+20	0.7863	1.84	824	-1.230	0.055
186.5739	51.7475	11.290	0.053	186.5983	51.7522	10.757	0.029	obv+20	0.5136	0.95	353	0.533	0.060
186.8958	17.1167	-8.000	5.000	186.8958	17.1167	-10.000	5.000	hbe09	0.5338	—	—	2.000	7.071
187.4627	45.9686	2.821	0.052	187.4664	46.0249	4.735	0.020	obv+20	0.3795	3.38	1055	-1.914†	0.056
188.4879	-35.5789	199.000	35.000	188.4879	-35.5789	-114.000	1.000	opa+17	0.1540*	—	—	313.000	35.014
188.6271	27.4074	4.219	0.009	188.6333	27.3587	5.939	0.006	obv+20	0.1589	2.94	484	-1.720	0.011
188.6479	53.3761	7.510	0.010	188.8529	53.2469	10.080	0.060	sob+20	0.3450*	10.68	3138	-2.570†	0.061
188.7563	53.2986	7.420	0.040	188.7563	53.2986	9.920	0.060	omv+19	0.3448*	—	—	-2.500	0.072
188.8477	21.3375	-3.900	1.200	188.8839	21.3489	-4.600	1.700	sc86	0.4220*	2.13	710	0.700	2.081
188.8555	53.2478	9.928	0.037	188.6481	53.3765	7.340	0.009	obv+20	0.0960	10.72	1145	2.588†	0.038
189.1583	12.9819	18.000	2.000	189.1583	12.9819	12.000	2.000	hbe09	0.3692	—	—	6.000	2.828
189.2079	46.0639	21.440	0.040	189.1900	46.0831	16.920	0.080	sob+20	0.6150*	1.37	556	4.520	0.089
190.0885	53.5813	17.765	0.005	190.0205	53.5743	19.183	0.004	obv+20	0.2926	2.46	647	-1.418	0.006
190.0900	53.5811	17.952	0.006	190.0271	53.5731	19.353	0.005	sob+20	0.2930*	2.29	602	-1.401	0.008
190.8147	43.2164	9.912	0.004	190.7805	43.2099	9.914	0.005	obv+20	0.3233	1.55	436	-0.002	0.006
190.9891	16.3836	-10.700	1.000	190.9904	16.3797	-8.500	3.500	sc86	0.5551*	0.24	93	-2.200	3.640
191.9868	42.8603	1.054	0.045	191.9987	42.8466	1.384	0.023	obv+20	0.6285	0.98	402	-0.330	0.051
192.3067	38.2737	-10.025	0.026	192.3054	38.2912	-9.546	0.014	obv+20	0.7065	1.05	452	-0.479	0.030
193.3984	15.7141	1.600	1.800	193.3848	15.7069	-13.600	14.800	prm+89	0.7660*	0.90	400	15.200	14.909
193.5496	27.6231	6.100	1.300	193.5508	27.6281	3.600	5.900	sc86	0.0853*	0.31	30	2.500	6.042
194.0375	21.7261	-8.000	2.000	194.0375	21.7261	-1.000	3.000	hbe09	0.5069	—	—	-7.000	3.606
194.2428	47.3389	-37.700	8.000	194.2376	47.3390	-7.500	4.000	gkb+04	0.9960*	0.21	101	-30.200	8.944
194.3358	-33.5781	-33.000	3.000	194.3358	-33.5781	-76.000	4.000	opa+17	0.1900*	—	—	43.000	5.000
194.6139	51.7090	4.787	0.029	194.5957	51.7041	5.195	0.024	obv+20	0.3941	0.74	237	-0.408	0.038
194.7774	36.5345	5.900	3.000	194.7736	36.5319	15.400	3.000	gkb+04	1.1270*	0.24	118	-9.500	4.243
194.8710	36.2877	-115.300	9.000	194.8796	36.2799	-115.600	10.000	gkb+04	1.0000*	0.62	298	0.300	13.454
195.3450	60.5170	9.573	0.046	195.3197	60.5154	8.716	0.017	obv+20	0.1975	0.75	147	0.857	0.049
195.3792	54.1300	13.676	0.009	195.4408	54.1450	14.017	0.004	sob+20	0.3130*	2.35	647	-0.341	0.010
195.5154	50.8950	6.632	0.022	195.5193	50.9000	6.970	0.027	obv+20	0.4978	0.34	124	-0.338	0.035
196.7653	52.6931	5.842	0.021	196.7802	52.6782	5.630	0.022	obv+20	0.3770	1.04	323	0.212	0.030

Table A1 *continued*

Table A1 (continued)

Source 1				Source 2									
RA1	Dec1	RM1	σ_{RM1}	RA2	Dec2	RM2	σ_{RM2}	Ref.	z	Δr	LS	ΔRM	$\sigma_{\Delta \text{RM}}$
(deg)	(deg)	(rad m ⁻²)		(deg)	(deg)	(rad m ⁻²)			(arcmin)	(kpc)		(rad m ⁻²)	
197.7391	27.4725	-2.400	1.700	197.7915	27.4642	-1.000	0.600	sc86	0.2398*	2.83	644	-1.400	1.803
199.1042	41.8583	-13.000	2.000	199.1042	41.8583	1.000	4.000	hbe09	0.4386	—	—	-14.000	4.472
200.1100	49.2839	10.850	0.060	200.1271	49.2769	10.900	0.080	sob+20	0.6840*	0.79	336	-0.050	0.100
201.5062	36.8036	6.600	2.000	201.5099	36.7989	4.300	1.500	sc86	0.0544	0.34	22	2.300	2.500
201.7949	28.8906	5.107	0.051	201.8191	28.8830	4.643	0.014	obv+20	0.2127	1.35	281	0.464	0.053
201.9342	41.8328	-5.372	0.011	201.8771	41.8401	-5.109	0.006	obv+20	0.2273	2.59	566	-0.263	0.013
202.1870	27.8890	5.854	0.012	202.2193	27.8563	5.834	0.006	obv+20	0.0911	2.60	265	0.020	0.013
202.6879	47.0524	17.200	0.800	202.6887	47.0580	10.000	2.000	mzf+15	0.6706	0.34	143	7.200	2.154
202.8203	44.3090	10.774	0.034	202.8226	44.3227	11.929	0.035	obv+20	0.2878	0.83	216	-1.155	0.049
202.8440	47.2226	10.700	0.400	202.8644	47.2170	6.000	0.500	mzf+15	0.2402	0.90	205	4.700	0.640
203.3984	30.1313	4.003	0.007	203.3694	30.1243	4.161	0.009	obv+20	0.2843	1.57	404	-0.158	0.011
203.4011	36.6046	4.089	0.017	203.3791	36.6118	3.822	0.006	obv+20	0.3156	1.14	316	0.267	0.018
204.8350	50.9819	9.050	0.060	204.8471	50.9369	8.220	0.080	sob+20	0.3160*	2.74	759	0.830	0.100
205.2592	49.2781	10.520	0.010	205.2658	49.2581	10.002	0.008	sob+20	0.7470*	1.23	541	0.518	0.013
205.2665	49.2566	9.818	0.009	205.2584	49.2766	10.400	0.014	obv+20	0.6144	1.24	503	-0.582	0.017
206.2308	39.8698	6.139	0.028	206.3045	39.8876	6.693	0.015	obv+20	0.2675	3.56	878	-0.554	0.032
206.8673	36.6469	2.683	0.028	206.8595	36.6543	2.248	0.009	obv+20	0.6104	0.59	239	0.435	0.029
208.3963	26.5084	4.538	0.018	208.3980	26.5559	3.497	0.006	obv+20	0.5000	2.85	1044	1.041†	0.019
208.4027	36.1312	7.559	0.025	208.4198	36.1386	7.756	0.015	obv+20	0.0265	0.94	30	-0.197	0.029
210.4590	59.1623	10.939	0.047	210.4764	59.1658	12.617	0.016	obv+20	0.5082	0.57	211	-1.678	0.050
210.7621	51.4561	19.410	0.010	210.7142	51.4581	17.620	0.040	sob+20	0.5180*	1.80	672	1.790	0.041
210.7700	51.7489	11.380	0.030	210.8508	51.7439	12.870	0.030	sob+20	0.4850*	3.02	1089	-1.490†	0.042
210.8542	51.7435	12.581	0.028	210.7672	51.7492	11.203	0.024	obv+20	0.5103	3.25	1204	1.378†	0.037
211.4142	54.1969	14.998	0.007	211.4279	54.1731	13.340	0.050	sob+20	0.7610*	1.51	669	1.658	0.050
211.7402	58.3804	12.929	0.036	211.7312	58.3666	11.643	0.016	obv+20	0.3507	0.88	261	1.286	0.039
213.5108	48.7069	19.940	0.020	213.5450	48.6939	19.180	0.080	sob+20	1.3610*	1.56	788	0.760	0.082
214.9282	54.3857	17.792	0.035	214.9453	54.3882	17.469	0.017	obv+20	0.7976	0.62	279	0.323	0.039
215.2743	41.7472	-126.300	8.000	215.2705	41.7458	16.000	5.000	gkb+04	0.3670*	0.19	58	-142.300	9.434
218.7920	41.8087	-4.690	0.013	218.7706	41.7847	-4.173	0.036	obv+20	0.4888	1.73	626	-0.517	0.038
219.9410	42.8158	-6.447	0.029	219.8695	42.8096	-5.349	0.065	obv+20	0.6877	3.17	1350	-1.098†	0.071
220.7253	53.9206	8.369	0.035	220.6966	53.9025	8.241	0.029	obv+20	0.5864	1.49	592	0.128	0.045
221.8065	42.6837	-9.628	0.046	221.8744	42.7276	-8.852	0.052	obv+20	0.1753	3.98	710	-0.776	0.069
222.2464	36.0570	2.455	0.050	222.2512	36.0470	2.566	0.024	obv+20	0.3410	0.64	187	-0.111	0.055
222.6622	36.2020	3.162	0.036	222.6375	36.1968	2.921	0.011	obv+20	0.2831	1.24	318	0.241	0.038
222.6900	53.0000	16.910	0.010	222.7608	53.0050	15.190	0.040	sob+20	0.9180*	2.58	1213	1.720†	0.041
223.9528	36.2324	5.804	0.029	223.9358	36.2424	5.423	0.008	obv+20	0.5196	1.02	381	0.381	0.030
224.4554	28.5143	8.450	0.010	224.4920	28.5599	5.527	0.005	obv+20	0.1440	3.35	508	2.923	0.011
224.9219	29.0644	19.137	0.028	224.9291	29.0544	18.063	0.026	obv+20	0.1381	0.71	104	1.074	0.038
224.9353	35.7742	0.875	0.053	224.9447	35.7891	0.931	0.046	obv+20	0.3612	1.01	306	-0.056	0.070
225.4654	43.7879	-6.739	0.021	225.4318	43.7413	-7.463	0.008	obv+20	0.4577	3.15	1100	0.724†	0.022
226.1521	50.5011	6.160	0.030	226.2250	50.5050	5.710	0.040	sob+20	0.6520*	2.79	1162	0.450†	0.050
229.4059	45.8318	-5.532	0.012	229.3970	45.8393	-4.940	0.007	obv+20	0.5180	0.59	220	-0.592	0.014
231.1438	45.6192	2.215	0.009	231.1813	45.6198	3.823	0.008	obv+20	0.3956	1.58	506	-1.608	0.012
231.3630	55.2405	-5.176	0.013	231.3695	55.2468	-5.523	0.008	obv+20	0.3991	0.44	142	0.347	0.015

Table A1 continued

Table A1 (*continued*)

Source 1				Source 2									
RA1	Dec1	RM1	σ_{RM1}	RA2	Dec2	RM2	σ_{RM2}	Ref.	z	Δr	LS	ΔRM	$\sigma_{\Delta \text{RM}}$
(deg)	(deg)	(rad m ⁻²)		(deg)	(deg)	(rad m ⁻²)				(arcmin)	(kpc)	(rad m ⁻²)	
231.9079	-30.2500	19.000	1.000	231.9079	-30.2500	-242.000	8.000	opa+17	0.9690*	—	—	261.000	8.062
232.1036	53.1887	1.397	0.025	232.1140	53.1749	2.336	0.033	obv+20	0.2160	0.91	191	-0.939	0.041
235.2534	59.2688	-4.725	0.052	235.2990	59.2578	-5.858	0.028	obv+20	0.4671	1.55	547	1.133	0.059
235.3491	49.1459	11.431	0.013	235.3835	49.1459	13.053	0.048	obv+20	0.2391	1.35	307	-1.622	0.050
237.4549	21.4276	22.100	4.000	237.4521	21.4268	43.000	5.000	gkb+04	1.2063*	0.16	80	-20.900	6.403
239.5418	29.1201	4.937	0.033	239.5490	29.1176	5.989	0.033	obv+20	0.2775	0.40	101	-1.052	0.047
240.0065	32.4372	5.151	0.062	240.0152	32.4560	5.082	0.017	obv+20	0.3197	1.21	338	0.069	0.064
240.9453	52.6953	19.362	0.020	240.9290	52.7141	21.619	0.010	obv+20	0.2919	1.27	333	-2.257	0.022
242.0609	35.2231	15.670	0.059	242.0532	35.2331	16.645	0.018	obv+20	2.3150	0.71	349	-0.975	0.062
243.6996	32.1865	5.982	0.035	243.7129	32.1778	6.487	0.022	obv+20	0.2239	0.86	186	-0.505	0.041
247.0247	27.7015	20.300	5.000	247.0092	27.6891	18.200	5.000	gkb+04	0.4480*	1.10	379	2.100	7.071
247.2250	44.3176	59.200	22.600	247.2083	44.3202	31.300	12.400	prm+89	0.6350*	0.73	301	27.900	25.778
254.3318	37.0603	26.892	0.054	254.3195	37.0705	26.306	0.032	obv+20	0.3913	0.85	271	0.586	0.063
255.2031	63.1288	-4.000	3.000	255.2031	63.1288	-11.000	11.000	pdb+11	0.5629	—	—	7.000	11.402
256.1810	60.7479	1.000	5.000	256.1638	60.7341	4.400	3.000	gkb+04	0.3719*	0.97	299	-3.400	5.831
256.5032	36.7083	15.088	0.058	256.4877	36.7147	15.527	0.046	obv+20	0.7477	0.84	370	-0.439	0.074
256.5433	64.6365	20.000	9.000	256.5433	64.6365	10.000	12.000	pdb+11	0.1729	—	—	10.000	15.000
260.2482	26.3962	63.062	0.032	260.3125	26.4199	60.452	0.040	obv+20	0.1696	3.73	648	2.610	0.051
261.0740	50.9728	25.100	2.200	261.0841	50.9539	16.400	5.600	prm+89	1.0790*	1.20	586	8.700	6.017
262.0984	64.3718	25.000	1.000	262.0984	64.3718	20.000	4.000	pdb+11	0.5174	—	—	5.000	4.123
263.6769	16.0116	-4.300	5.000	263.6778	16.0075	0.900	3.000	gkb+04	1.2960*	0.26	131	-5.200	5.831
264.3642	-56.6031	24.968	0.139	264.4429	-56.5419	48.352	0.039	rgs+20	0.0980*	4.50	489	-23.384	0.144
270.3167	69.0465	44.800	3.000	270.3056	69.0421	20.800	2.000	gkb+04	1.2710*	0.36	181	24.000	3.606
271.2770	11.0266	38.500	8.800	271.2764	11.0247	80.500	1.400	prm+89	1.1310*	0.12	59	-42.000	8.911
273.2037	68.7994	13.900	3.000	273.1713	68.7895	-68.400	7.000	gkb+04	1.0300*	0.92	445	82.300	7.616
274.6803	41.8704	43.400	0.022	274.6892	41.8840	43.704	0.016	obv+20	0.5509	0.91	351	-0.304	0.027
276.0911	63.5914	36.368	0.020	276.1165	63.6001	37.909	0.024	obv+20	0.4609	0.86	301	-1.541	0.031
278.8204	62.0447	55.756	0.008	278.7613	62.0936	59.537	0.006	obv+20	0.5194	3.37	1260	-3.781†	0.010
278.9348	42.0610	25.391	0.031	278.9264	42.0572	26.091	0.017	obv+20	0.3556	0.44	132	-0.700	0.035
305.0221	29.7089	-174.000	4.000	305.0279	29.7025	552.000	4.000	ccsk92	0.2485*	0.49	115	-726.000†	5.657
308.9808	42.3019	298.000	9.000	308.9925	42.2900	-241.000	4.000	ccsk92	0.1741	0.88	156	539.000†	9.849
316.7423	-24.0865	-10.000	2.100	316.7423	-24.0865	5.700	7.000	akm+98	2.4910*	—	—	-15.700	7.308
319.5650	60.7933	14.200	2.500	319.5912	60.8128	-79.800	5.700	sc86	0.0555*	1.40	91	94.000†	6.224
325.5695	-28.9779	-49.800	2.000	325.5695	-28.9779	10.300	1.700	akm+98	2.5500*	—	—	-60.100	2.625
327.8736	5.8091	-37.324	0.056	327.8535	5.8154	-36.218	0.022	obv+20	0.6080	1.26	509	-1.106	0.060
328.1108	-34.2684	-96.000	2.000	328.1108	-34.2684	19.000	4.000	bbh+07	1.2770*	—	—	-115.000	4.472
328.9662	38.0064	-349.200	36.400	328.9662	38.0094	-344.700	37.800	sc86	0.2900*	—	—	-4.500	52.477
331.5187	29.4914	-128.600	3.600	331.5237	29.4844	-131.200	1.200	sc86	0.7080*	0.49	211	2.600	3.795
341.6266	36.9411	-245.000	2.100	341.6282	36.9428	-219.900	2.500	sc86	0.0816*	0.13	12	-25.100	3.265
345.3155	19.6672	-49.008	0.016	345.3301	19.6772	-51.106	0.025	obv+20	0.4267	1.02	342	2.098	0.030
346.1954	27.0541	-53.138	0.015	346.1758	27.0543	-53.524	0.007	obv+20	0.6170	1.05	427	0.386	0.017
352.8482	22.8573	-40.036	0.006	352.8797	22.8401	-40.091	0.011	obv+20	0.2360	2.02	454	0.055	0.013
358.0854	33.0736	-61.700	1.600	358.0929	33.0583	-65.500	1.100	sc86	0.6590*	0.99	414	3.800	1.942
359.0958	79.9318	17.300	8.100	358.8558	79.9116	7.600	7.900	prm+89	1.3360*	2.80	1412	9.700†	11.315

Table A1 *continued*

Table A1 (*continued*)

Source 1				Source 2				Ref.	z	Δr	LS	ΔRM	$\sigma_{\Delta RM}$						
RA1	Dec1	RM1	σ_{RM1}	RA2	Dec2	RM2	σ_{RM2}												
(deg)	(deg)	(rad m $^{-2}$)		(deg)	(deg)	(rad m $^{-2}$)													
Column 1 and 2: Equatorial coordinate of source 1; column 3 and 4: RM values and errors of source 1; column 5 and 6: Equatorial coordinate of source 2; column 7 and 8: RM values and errors of source 2; column 9: reference; column 10: redshift of double radio sources; column 11 and 12: angular separation (Δr) and projected linear separation (LS) of double radio sources; column 13 and 14: RM differences and uncertainties of double radio sources.																			
In column 10, values marked with '*' signify reliable redshift information from the original references.																			
In column 11 and 12, '-' means values are not available.																			
In column 13, values marked with '†' signify sources removed from the final sample used for the analysis.																			
The references are: akm+98, Athreya et al. (1998); bbh+07, Broderick et al. (2007); bowe19, Banfield et al. (2019); ccsk92, Clegg et al. (1992); gkb+04, Goodlet et al. (2004); hbb98, Han et al. (1998); hbe09, Heald et al. (2009); ms96, Minter & Spangler (1996); obv+20, O'Sullivan et al. (2020); omv+19, O'Sullivan et al. (2019); opa+17, O'Sullivan et al. (2017); prm+89, Pedelty et al. (1989); rgs+20, Rieseley et al. (2020); sc86, Simonetti & Cordes (1986); sob+20, Stuardi et al. (2020); tss09, Taylor et al. (2009).																			

Table A2. 401 double radio sources with RM and redshift data from the NVSS data. Columns are the same as Table A1.

Source 1				Source 2				Ref.	z	Δr	LS	ΔRM	$\sigma_{\Delta RM}$
RA1	Dec1	RM1	σ_{RM1}	RA2	Dec2	RM2	σ_{RM2}						
(deg)	(deg)	(rad m $^{-2}$)		(deg)	(deg)	(rad m $^{-2}$)							
0.2804	23.8897	-73.200	13.300	0.2815	23.8724	-64.800	4.600	tss09	0.4576	1.04	363	-8.400	14.073
0.9972	-23.1163	15.700	6.400	1.0258	-23.1171	19.100	12.900	tss09	0.0970	1.58	170	-3.400	14.400
2.6788	-6.0596	23.800	10.300	2.6957	-6.0677	5.300	5.800	tss09	0.0417	1.12	55	18.500	11.821
3.3116	20.7924	-37.900	14.900	3.3344	20.7969	-26.100	3.300	tss09	0.2827	1.30	334	-11.800	15.261
4.0463	32.6553	14.600	13.100	4.0554	32.6443	-32.600	7.000	tss09	0.8395	0.81	371	47.200	14.853
4.5512	21.7087	-45.900	11.900	4.5731	21.6771	-51.600	9.700	tss09	0.3026	2.26	608	5.700	15.353
5.0840	-20.4925	-13.800	12.900	5.0948	-20.4698	-11.500	4.800	tss09	0.5450	1.49	571	-2.300	13.764
5.1949	23.8077	-48.900	12.400	5.1979	23.7923	-38.100	12.700	tss09	0.5024	0.94	345	-10.800	17.750
5.4690	-12.5655	7.100	5.500	5.4824	-12.5699	43.900	15.600	tss09	0.6215	0.83	339	-36.800	16.541
5.7818	-25.0384	-3.400	1.400	5.7969	-25.0484	6.800	2.600	tss09	0.3500	1.02	302	-10.200	2.953
6.5487	11.6573	-7.200	10.400	6.5627	11.7657	-9.400	7.300	tss09	0.7133	6.56	2835	2.200†	12.706
8.4177	4.2149	2.700	10.100	8.4468	4.2007	0.100	16.100	tss09	0.6791	1.94	822	2.600	19.006
8.9942	-3.8628	-23.300	7.400	9.0082	-3.8739	-1.200	7.300	tss09	0.7527	1.07	472	-22.100	10.395
9.4322	38.8014	-99.600	1.700	9.4593	38.7961	-95.100	16.800	tss09	0.4841	1.31	472	-4.500	16.886
9.5305	9.5769	-2.500	13.200	9.5536	9.6280	-20.900	16.600	tss09	0.2942	3.36	886	18.400	21.208
9.5769	-18.8644	-2.900	4.000	9.6025	-18.8688	-3.400	13.200	tss09	0.3375	1.48	429	0.500	13.793
11.0080	1.0083	-11.800	17.800	11.0297	1.0502	-10.000	9.100	tss09	0.1117	2.83	345	-1.800	19.991
13.1043	12.3307	6.500	5.000	13.1136	12.3190	8.300	10.100	tss09	0.7118	0.89	384	-1.800	11.270
14.3923	-1.3829	3.600	0.600	14.3982	-1.4018	6.600	4.200	tss09	0.0450	1.19	63	-3.000	4.243
14.5481	4.1071	-5.800	14.200	14.5513	4.1246	-18.600	6.500	tss09	0.5748	1.07	421	12.800	15.617
15.5596	2.0621	-18.500	2.600	15.5675	2.0451	-19.600	1.700	tss09	0.5228	1.12	420	1.100	3.106
16.3842	28.6092	-41.600	5.100	16.4124	28.6251	-48.300	22.600	tss09	0.1234	1.77	235	6.700	23.168
16.5404	24.8612	-35.100	9.300	16.5507	24.8456	-46.600	5.300	tss09	0.6271	1.09	446	11.500	10.704
16.9931	26.9886	-37.400	7.600	17.0348	27.0165	-35.600	28.200	tss09	0.2580	2.78	668	-1.800	29.206
17.1838	15.5434	-16.400	9.700	17.2033	15.5671	-19.600	15.100	tss09	0.2919	1.82	478	3.200	17.947
18.4117	1.1059	13.200	11.400	18.4368	1.0918	7.700	8.700	tss09	0.5785	1.73	682	5.500	14.341

Table A2 *continued*

Table A2 (continued)

Source 1				Source 2									
RA1 (deg)	Dec1 (deg)	RM1 (rad m ⁻²)	σ_{RM1}	RA2 (deg)	Dec2 (deg)	RM2 (rad m ⁻²)	σ_{RM2}	Ref.	z	Δr (arcmin)	LS (kpc)	ΔRM	$\sigma_{\Delta \text{RM}}$
19.5870	47.1919	-82.400	4.600	19.6003	47.2158	-78.100	4.300	tss09	0.5934	1.54	615	-4.300	6.297
21.2692	27.7208	-50.800	10.200	21.2920	27.7433	-52.500	10.100	tss09	0.6073	1.81	730	1.700	14.354
21.8131	2.1377	7.700	2.300	21.8144	2.1526	-0.500	5.000	tss09	0.2130	0.89	185	8.200	5.504
22.4997	-9.6667	10.900	15.800	22.5002	-9.6507	-7.600	13.000	tss09	0.3590	0.96	289	18.500	20.461
23.3615	29.0110	-52.900	16.100	23.3650	28.9923	-45.100	11.800	tss09	0.2447	1.14	263	-7.800	19.961
23.8409	-5.2826	-12.100	10.200	23.8580	-5.2730	-5.600	2.200	tss09	0.3138	1.17	323	-6.500	10.435
24.0968	20.9493	-11.600	0.900	24.1059	20.9635	40.200	5.200	tss09	0.4266	0.99	332	-51.800	5.277
24.1002	-4.0802	-6.100	15.500	24.1227	-4.0722	-4.700	17.500	tss09	0.5690	1.43	560	-1.400	23.377
24.7314	57.3332	-43.100	4.400	24.7590	57.3433	-46.800	5.000	tss09	0.5752	1.08	425	3.700†	6.660
24.8827	-8.8356	-7.500	6.300	24.8930	-8.8459	3.900	6.200	tss09	0.4559	0.87	303	-11.400	8.839
25.7214	54.5421	-62.300	6.000	25.7462	54.5421	-47.700	13.900	tss09	0.0647	0.86	64	-14.600†	15.140
25.9438	-2.2700	16.600	9.200	25.9590	-2.2734	2.100	10.200	tss09	0.1721	0.94	165	14.500	13.736
26.8255	-8.8582	-7.500	11.700	26.8383	-8.8484	-10.400	6.500	tss09	0.4547	0.96	334	2.900	13.384
27.0273	-0.9275	7.900	6.700	27.0457	-0.9333	-9.700	10.700	tss09	0.8021	1.16	523	17.600	12.625
28.5074	-14.9797	14.000	12.300	28.5207	-14.9521	2.000	9.400	tss09	0.6053	1.82	733	12.000	15.481
29.1349	21.0398	-34.300	7.300	29.1579	21.0700	-37.200	10.700	tss09	0.6631	2.22	931	2.900	12.953
29.2845	28.8619	-109.300	9.000	29.3035	28.8606	-108.800	1.000	tss09	0.5816	1.00	396	-0.500	9.055
30.2257	61.6050	-172.500	8.900	30.2572	61.5998	-128.600	12.800	tss09	0.3520	0.95	283	-43.900†	15.590
31.5142	-5.1902	16.100	4.500	31.5269	-5.1952	4.500	14.600	tss09	0.5742	0.82	322	11.600	15.278
31.6105	-3.7481	14.600	5.500	31.6145	-3.7346	11.900	4.500	tss09	0.4824	0.85	306	2.700	7.106
32.2627	7.8381	15.200	4.800	32.2743	7.8313	6.300	5.600	tss09	0.2580	0.80	192	8.900	7.376
32.5500	15.5414	-12.600	2.700	32.5690	15.5472	-13.300	2.700	tss09	0.3798	1.16	362	0.700	3.818
33.5247	32.8372	-57.700	13.700	33.6132	32.8688	-71.400	5.600	tss09	0.1643	4.85	821	13.700	14.800
33.8974	-12.9915	5.600	0.700	33.9130	-12.9926	12.400	0.600	tss09	0.1470	0.91	140	-6.800	0.922
34.1470	2.7252	-7.100	2.900	34.1510	2.7411	-16.800	2.900	tss09	0.1782	0.99	179	9.700	4.101
34.7603	-36.4284	-4.000	4.800	34.7632	-36.4459	12.800	8.500	tss09	0.4888	1.06	384	-16.800	9.762
38.1570	-1.0676	-8.300	11.400	38.1625	-1.0887	-5.400	5.500	tss09	0.2966	1.31	348	-2.900	12.657
39.2498	-28.5728	5.300	2.400	39.2583	-28.5928	10.300	5.900	tss09	0.1444	1.28	195	-5.000	6.369
40.1349	-15.9532	18.300	17.100	40.1567	-15.9482	25.700	12.900	tss09	0.4773	1.30	465	-7.400	21.420
42.5439	39.5777	-50.100	9.000	42.5877	39.5736	-31.700	10.200	tss09	0.2040	2.04	410	-18.400	13.603
43.9548	-20.4603	4.100	1.000	43.9791	-20.4657	7.300	6.700	tss09	0.6900	1.40	597	-3.200	6.774
44.2567	-6.1330	27.400	7.400	44.2628	-6.1498	14.400	5.400	tss09	0.3489	1.07	317	13.000	9.161
44.2885	6.6287	-7.800	1.400	44.3026	6.6377	26.600	8.100	tss09	0.1502	1.00	157	-34.400	8.220
44.9065	13.9102	-9.400	4.400	44.9139	13.9234	-4.200	4.000	tss09	0.0748	0.90	77	-5.200	5.946
46.8778	-22.4154	-100.700	11.600	46.8862	-22.4303	1.700	1.300	tss09	0.2680	1.01	249	-102.400	11.673
50.5792	17.7859	-15.400	7.100	50.5969	17.8105	-12.800	1.900	tss09	0.2173	1.79	378	-2.600	7.350
53.8299	-6.9463	2.200	6.300	53.8387	-6.9313	4.100	2.400	tss09	0.1991	1.04	205	-1.900	6.742
54.8607	38.9618	71.400	10.400	54.8836	38.9606	69.100	9.600	tss09	0.5207	1.07	401	2.300	14.153
56.1200	17.4831	36.800	16.600	56.1468	17.4915	11.000	9.000	tss09	0.4063	1.62	528	25.800	18.883
56.9950	40.7270	81.300	1.000	57.0050	40.7400	80.100	1.100	tss09	0.0390	0.90	42	1.200	1.487
60.6820	-18.0004	-3.700	2.500	60.6905	-18.0160	-10.600	4.500	tss09	0.3410	1.05	306	6.900	5.148
63.4133	11.2129	-26.000	2.700	63.4256	11.1958	-11.300	2.000	tss09	0.3056	1.25	339	-14.700	3.360
63.6184	14.2801	-45.700	1.600	63.6303	14.2656	-49.500	1.500	tss09	0.1803	1.11	203	3.800	2.193
64.9193	31.5979	66.800	5.800	64.9401	31.5931	74.200	12.300	tss09	0.5555	1.10	425	-7.400	13.599

Table A2 continued

Table A2 (continued)

Source 1				Source 2									
RA1	Dec1	RM1	σ_{RM1}	RA2	Dec2	RM2	σ_{RM2}	Ref.	z	Δr	LS	ΔRM	$\sigma_{\Delta \text{RM}}$
(deg)	(deg)	(rad m $^{-2}$)		(deg)	(deg)	(rad m $^{-2}$)			(arcmin)	(kpc)	(rad m $^{-2}$)		
65.4806	-0.0677	-24.000	12.100	65.4920	-0.0747	-14.100	13.500	tss09	0.3982	0.80	257	-9.900	18.129
67.5474	77.3785	-28.800	15.100	67.8673	77.3897	-39.400	20.000	tss09	0.2150	4.25	891	10.600	25.060
67.5673	-28.0133	32.300	1.600	67.5846	-28.0108	34.100	2.200	tss09	0.6500	0.93	387	-1.800	2.720
71.1510	-28.1562	29.800	2.700	71.1607	-28.1702	36.500	3.300	tss09	0.1470	0.98	151	-6.700	4.264
78.4833	17.0842	-26.100	8.100	78.5176	17.0900	-55.500	16.800	tss09	0.2417	1.99	456	29.400	18.651
80.6211	0.8841	31.000	5.500	80.6419	0.9014	31.400	14.700	tss09	0.7845	1.62	725	-0.400	15.695
82.7605	0.3750	29.700	9.000	82.7730	0.3894	15.100	10.900	tss09	0.4359	1.14	387	14.600	14.135
84.0296	5.4764	-9.200	20.300	84.0393	5.5052	9.200	5.900	tss09	0.3599	1.82	550	-18.400	21.140
84.4224	19.8811	-29.700	9.000	84.4260	19.8946	-34.900	8.100	tss09	0.4911	0.84	305	5.200 \dagger	12.108
85.5631	19.8589	-51.000	7.800	85.5695	19.8410	-44.800	16.600	tss09	0.6021	1.13	454	-6.200 \dagger	18.341
85.8222	-12.1878	-26.300	10.900	85.8300	-12.1706	-26.900	4.800	tss09	0.0798	1.13	102	0.600	11.910
94.5135	0.5574	59.400	10.600	94.5135	0.5829	52.900	7.800	tss09	0.4416	1.53	523	6.500 \dagger	13.161
94.9877	-37.1954	5.800	6.900	95.0147	-37.1919	-0.500	3.200	tss09	0.0328	1.31	51	6.300	7.606
102.7375	15.3147	55.900	5.800	102.7550	15.3128	80.100	4.500	tss09	0.0565	1.02	67	-24.200 \dagger	7.341
105.5307	25.2187	10.800	7.600	105.5379	25.2419	30.000	5.500	tss09	0.5191	1.45	542	-19.200	9.381
106.8753	82.6008	-4.600	18.500	107.2757	82.6280	-12.000	21.300	tss09	0.2184	3.49	740	7.400	28.212
108.9415	65.9792	-15.600	16.400	108.9620	65.9926	-33.600	8.700	tss09	0.6150	0.94	382	18.000	18.565
110.9702	65.0907	-18.200	2.300	110.9902	65.0780	-23.000	2.300	tss09	0.2184	0.91	193	4.800	3.253
111.2021	16.0216	20.500	5.100	111.2190	16.0319	24.300	3.300	tss09	0.3092	1.15	314	-3.800	6.075
111.5270	32.6312	-12.800	13.100	111.5360	32.6117	-1.700	6.000	tss09	0.7326	1.26	550	-11.100	14.409
111.7689	-2.0894	49.200	10.700	111.7712	-2.0682	45.600	2.200	tss09	0.2200	1.28	273	3.600 \dagger	10.924
112.0069	50.5826	-4.400	2.000	112.0437	50.5744	4.700	9.200	tss09	0.3500	1.49	442	-9.100	9.415
113.3011	42.2149	-0.600	7.800	113.3123	42.1845	-2.700	12.300	tss09	0.0664	1.89	144	2.100	14.565
115.3299	20.8409	41.700	7.500	115.3346	20.8548	30.200	5.700	tss09	0.8162	0.87	395	11.500	9.420
115.3509	33.5696	6.700	10.900	115.3599	33.5396	-0.400	7.000	tss09	0.3636	1.85	562	7.100	12.954
115.6730	48.8885	25.800	6.800	115.6965	48.8865	30.500	8.300	tss09	0.4343	0.93	315	-4.700	10.730
117.1730	8.0319	-28.100	7.600	117.1864	8.0221	-27.500	8.500	tss09	0.4482	0.99	342	-0.600	11.402
117.2300	33.4721	17.400	10.100	117.2554	33.4740	8.400	9.900	tss09	0.4550	1.28	445	9.000	14.143
120.0175	32.0356	14.200	13.500	120.0343	32.0259	-6.200	7.000	tss09	0.4648	1.03	363	20.400	15.207
120.3004	19.2730	19.400	7.500	120.3048	19.2553	21.700	8.400	tss09	0.4085	1.09	356	-2.300	11.261
120.4963	63.8927	-16.100	9.300	120.5184	63.8788	-20.800	3.900	tss09	0.4721	1.02	362	4.700	10.085
120.9252	9.9540	32.200	8.400	120.9373	9.9658	35.000	5.400	tss09	0.0717	1.01	83	-2.800	9.986
122.0675	49.4849	3.400	4.100	122.0727	49.4622	14.300	15.600	tss09	0.1985	1.37	270	-10.900	16.130
122.3633	22.3256	29.400	17.600	122.3701	22.3151	30.900	11.700	tss09	0.7714	0.74	329	-1.500	21.134
124.3190	17.6939	31.600	5.300	124.3225	17.6702	26.900	13.800	tss09	0.2167	1.44	304	4.700	14.783
124.9102	23.1771	3.700	10.600	124.9246	23.1637	15.800	8.800	tss09	0.6417	1.13	467	-12.100	13.777
126.2562	12.7321	30.800	9.100	126.2832	12.7370	28.900	5.200	tss09	0.3216	1.61	451	1.900	10.481
126.5550	45.6057	13.200	13.300	126.5602	45.5907	6.000	6.900	tss09	0.5770	0.93	366	7.200	14.983
127.9856	13.8717	23.100	5.800	127.9963	13.8876	26.000	2.300	tss09	0.6134	1.14	462	-2.900	6.239
128.3308	11.5208	41.400	3.700	128.3422	11.5156	44.500	4.900	tss09	0.6176	0.74	301	-3.100	6.140
130.7878	29.7262	10.800	2.300	130.7945	29.7429	7.400	4.300	tss09	0.3980	1.06	341	3.400	4.876
131.6359	14.2239	24.700	9.000	131.6681	14.2128	21.200	13.300	tss09	0.4929	1.99	724	3.500	16.059
131.6982	20.3900	27.000	7.100	131.7003	20.4111	30.800	10.000	tss09	0.6723	1.27	536	-3.800	12.264
132.8419	49.0026	-7.400	7.800	132.8683	48.9821	-12.800	3.200	tss09	0.4891	1.61	583	5.400	8.431

Table A2 continued

Table A2 (continued)

Source 1				Source 2									
RA1	Dec1	RM1	σ_{RM1}	RA2	Dec2	RM2	σ_{RM2}	Ref.	z	Δr	LS	ΔRM	$\sigma_{\Delta RM}$
(deg)	(deg)	(rad m $^{-2}$)		(deg)	(deg)	(rad m $^{-2}$)			(arcmin)	(kpc)	(rad m $^{-2}$)		
133.5045	7.4288	61.700	10.800	133.5112	7.4138	45.800	15.900	tss09	0.2260	0.98	213	15.900	19.221
133.6418	14.6662	55.000	13.600	133.6555	14.6750	41.000	11.500	tss09	0.6095	0.95	384	14.000	17.810
133.9122	18.8127	20.800	12.000	133.9274	18.7933	38.600	12.000	tss09	0.5551	1.45	561	-17.800	16.971
134.1154	59.9686	-15.900	12.900	134.1682	59.9561	-6.500	16.900	tss09	0.2830	1.75	449	-9.400	21.261
134.3163	9.8141	2.200	4.100	134.3271	9.8007	-2.100	3.500	tss09	2.7350	1.03	488	4.300	5.391
134.6246	8.0660	3.300	8.500	134.6314	8.0806	9.900	9.800	tss09	0.4549	0.96	334	-6.600	12.973
135.0342	61.5712	-7.900	17.100	135.0911	61.5692	-15.000	15.800	tss09	0.7781	1.63	728	7.100	23.282
137.1401	48.6611	-1.300	7.500	137.1596	48.6484	2.000	11.400	tss09	0.1167	1.09	138	-3.300	13.646
138.6884	41.6276	-2.400	1.800	138.6919	41.6100	-2.900	3.100	tss09	0.1404	1.06	157	0.500	3.585
139.0257	31.8227	39.500	12.600	139.0411	31.8168	32.800	10.700	tss09	0.3905	0.86	273	6.700	16.530
141.9840	27.6403	20.500	14.400	142.0053	27.6421	9.400	3.000	tss09	0.6821	1.13	480	11.100	14.709
142.8919	51.4467	13.300	15.600	142.9348	51.4559	-9.600	12.900	tss09	0.5795	1.70	671	22.900	20.243
143.1780	7.5482	17.200	7.400	143.1847	7.5698	38.300	15.800	tss09	0.2892	1.35	352	-21.100	17.447
143.3385	43.7273	-9.600	15.600	143.3460	43.7135	-0.100	16.100	tss09	0.3919	0.89	284	-9.500	22.418
144.7188	25.9718	6.900	7.400	144.7266	25.9919	4.800	3.100	tss09	0.2374	1.28	289	2.100	8.023
145.1370	11.5196	11.600	7.100	145.1450	11.5358	9.200	6.600	tss09	0.0753	1.07	92	2.400	9.694
145.2075	-20.7862	-66.200	8.700	145.2137	-20.8002	-51.500	4.000	tss09	0.3710	0.91	280	-14.700	9.575
145.2474	31.4275	16.000	4.800	145.2798	31.4488	4.500	8.400	tss09	0.2583	2.09	503	11.500	9.675
145.3484	39.7373	3.900	2.500	145.3516	39.7541	-7.500	1.200	tss09	0.1075	1.02	120	11.400	2.773
145.7586	28.5879	15.400	3.600	145.7588	28.5667	15.000	7.400	tss09	0.5742	1.27	499	0.400	8.229
148.2714	8.7237	36.800	8.500	148.2820	8.7393	24.900	6.100	tss09	0.7053	1.12	482	11.900	10.462
148.5168	21.3745	28.900	11.200	148.5406	21.3792	5.500	3.600	tss09	0.2956	1.36	360	23.400	11.764
149.4679	31.8467	18.100	7.000	149.5002	31.8405	14.700	12.500	tss09	0.1800	1.69	308	3.400	14.327
149.6263	56.3376	8.500	7.500	149.6502	56.3196	15.700	7.500	tss09	0.2260	1.34	292	-7.200	10.607
149.7811	64.1390	2.700	11.000	149.8184	64.1395	5.700	11.700	tss09	0.7518	0.98	432	-3.000	16.059
150.3391	-0.4385	8.600	1.300	150.3519	-0.4341	2.100	1.200	tss09	0.4106	0.81	265	6.500	1.769
150.4654	-0.8689	-6.700	4.500	150.4784	-0.8881	-10.200	9.600	tss09	0.1364	1.39	201	3.500	10.602
151.1901	22.4151	14.200	5.600	151.1909	22.4312	26.000	10.900	tss09	0.9806	0.97	464	-11.800	12.254
152.7150	-2.0409	10.400	14.200	152.7157	-2.0053	-15.400	8.700	tss09	0.7088	2.14	923	25.800	16.653
153.9712	40.7781	13.400	7.200	154.0079	40.7826	11.600	3.400	tss09	0.1279	1.69	232	1.800	7.962
154.7892	15.8280	5.600	8.400	154.8039	15.8364	-3.500	5.800	tss09	0.4969	0.98	358	9.100	10.208
155.0035	-2.7821	6.400	15.900	155.0233	-2.7960	-34.000	12.600	tss09	1.4467	1.45	735	40.400	20.287
156.4056	37.3409	5.400	17.100	156.4166	37.3259	-17.100	15.500	tss09	0.6533	1.04	434	22.500	23.079
156.8110	46.0389	8.200	1.800	156.8124	46.0561	-0.900	1.600	tss09	0.5264	1.03	388	9.100	2.408
157.2465	-20.4641	-58.400	2.700	157.2479	-20.4490	-64.300	2.200	tss09	0.5660	0.91	355	5.900	3.483
157.2612	64.9668	-24.700	3.900	157.3126	64.9579	-26.000	7.800	tss09	0.3859	1.41	445	1.300	8.721
158.9708	2.8234	29.000	6.400	158.9741	2.8382	16.700	7.600	tss09	0.2897	0.91	238	12.300	9.936
159.0083	20.1709	6.900	10.000	159.0296	20.1983	-5.400	20.900	tss09	0.0423	2.04	102	12.300	23.169
159.0451	-25.4293	3.200	3.800	159.0531	-25.4121	2.800	4.800	tss09	0.4400	1.12	382	0.400	6.122
159.4487	15.6851	37.900	7.400	159.4588	15.6949	61.600	12.100	tss09	0.1958	0.83	162	-23.700	14.183
159.7247	57.8854	-1.600	5.800	159.7460	57.8719	15.300	14.700	tss09	0.1008	1.06	118	-16.900	15.803
159.8588	5.6024	12.800	7.700	159.8779	5.6056	14.000	21.800	tss09	0.0908	1.15	117	-1.200	23.120
160.2083	33.1218	16.400	6.000	160.2165	33.1080	26.100	11.000	tss09	0.6177	0.92	374	-9.700	12.530
160.7627	39.2331	12.000	10.300	160.7824	39.2436	25.300	9.100	tss09	0.5947	1.11	444	-13.300	13.744

Table A2 continued

Table A2 (continued)

Source 1				Source 2									
RA1	Dec1	RM1	σ_{RM1}	RA2	Dec2	RM2	σ_{RM2}	Ref.	z	Δr	LS	ΔRM	$\sigma_{\Delta \text{RM}}$
(deg)	(deg)	(rad m $^{-2}$)		(deg)	(deg)	(rad m $^{-2}$)			(arcmin)	(kpc)	(rad m $^{-2}$)		
161.1382	14.7024	5.000	14.700	161.1542	14.6986	-30.100	5.100	tss09	0.1547	0.95	153	35.100	15.560
161.5752	54.9938	10.400	12.400	161.5969	54.9700	7.400	3.700	tss09	0.3570	1.61	484	3.000	12.940
161.6456	17.8647	6.600	12.600	161.6624	17.8641	19.300	12.100	tss09	0.6181	0.96	391	-12.700	17.469
162.8667	-9.2979	-17.100	5.800	162.8852	-9.3089	-7.500	2.200	tss09	0.3453	1.28	376	-9.600	6.203
164.0050	19.4011	-3.100	8.800	164.0207	19.4079	11.100	14.900	tss09	0.5577	0.97	376	-14.200	17.305
164.2464	58.7952	15.900	7.200	164.2777	58.7827	12.800	5.600	tss09	0.8305	1.23	561	3.100	9.121
165.0084	30.4617	10.300	1.800	165.0300	30.4429	8.800	3.200	tss09	0.6188	1.59	647	1.500	3.672
165.8414	20.8092	-18.100	5.000	165.8440	20.7919	-21.300	5.900	tss09	0.6411	1.05	434	3.200	7.734
166.6676	5.7801	35.300	9.800	166.6706	5.7607	5.300	12.000	tss09	0.2794	1.18	300	30.000	15.493
166.6991	27.7086	9.500	8.400	166.7060	27.7241	-13.700	13.200	tss09	0.4849	1.00	360	23.200	15.646
167.4489	37.6379	5.500	2.900	167.4669	37.6455	2.900	2.400	tss09	0.3454	0.97	285	2.600	3.764
168.1598	43.4409	81.700	2.200	168.1664	43.4274	64.600	6.300	tss09	0.3299	0.86	245	17.100	6.673
169.1881	25.8068	-13.000	10.600	169.2054	25.7996	9.500	5.100	tss09	0.2115	1.03	213	-22.500	11.763
171.5242	50.3895	9.500	12.000	171.5252	50.3716	5.700	5.000	tss09	0.4261	1.08	362	3.800	13.000
171.6727	10.7291	-11.900	10.500	171.6920	10.7134	-4.500	5.500	tss09	0.4475	1.48	510	-7.400	11.853
172.1021	58.5399	13.100	7.500	172.1405	58.5282	-3.400	11.000	tss09	0.4369	1.39	473	16.500	13.314
172.3420	21.0183	-1.600	7.700	172.3578	21.0256	-8.600	3.800	tss09	0.1076	0.99	117	7.000	8.587
172.7575	61.2540	12.700	1.900	172.7981	61.2499	21.900	6.300	tss09	0.3499	1.20	356	-9.200	6.580
173.5838	30.7663	2.000	2.200	173.5839	30.7861	8.000	6.500	tss09	0.2741	1.19	299	-6.000	6.862
173.9313	24.4283	30.600	12.800	173.9504	24.4166	13.500	6.300	tss09	0.3452	1.26	370	17.100	14.266
173.9546	25.9494	9.300	4.000	173.9566	25.9623	15.700	4.000	tss09	0.7123	0.78	337	-6.400	5.657
175.2142	25.4249	18.900	8.000	175.2397	25.4404	6.500	7.200	tss09	0.5932	1.67	667	12.400	10.763
175.2447	-12.3869	-13.400	8.500	175.2501	-12.4056	-7.600	8.100	tss09	0.0744	1.17	99	-5.800	11.741
176.1134	8.2385	26.300	4.000	176.1252	8.2286	39.500	8.100	tss09	0.3011	0.92	247	-13.200	9.034
176.2643	53.6492	8.700	5.700	176.2947	53.6482	12.200	9.900	tss09	0.0690	1.08	86	-3.500	11.424
176.3403	27.8549	-1.600	7.700	176.3586	27.8481	2.400	9.800	tss09	0.3694	1.06	325	-4.000	12.463
176.4916	29.3517	-23.200	16.900	176.5105	29.3537	2.100	15.000	tss09	0.3285	0.99	282	-25.300	22.597
176.6038	73.4509	-29.000	8.800	176.6679	73.4635	-41.100	12.500	tss09	0.3156	1.33	368	12.100	15.287
176.6298	-33.0060	-35.100	5.000	176.6524	-33.0080	-32.700	3.600	tss09	0.0602	1.14	80	-2.400	6.161
177.5287	57.9740	11.500	12.400	177.5373	57.9456	23.600	7.100	tss09	0.6193	1.73	704	-12.100	14.289
178.0283	21.3983	31.400	5.800	178.0395	21.3826	-18.400	15.500	tss09	0.1721	1.13	199	49.800	16.550
178.0731	24.5310	32.600	2.300	178.0918	24.5456	34.600	7.900	tss09	0.3055	1.35	366	-2.000	8.228
178.1841	8.2737	-2.100	5.500	178.2038	8.2653	-11.500	5.600	tss09	0.1204	1.28	167	9.400	7.849
178.4615	38.1962	-3.500	4.000	178.4786	38.1971	15.800	4.900	tss09	0.1981	0.81	159	-19.300	6.325
178.8074	65.6539	12.000	4.100	178.8452	65.6549	29.400	6.000	tss09	1.1978	0.94	468	-17.400	7.267
179.2859	5.3011	8.100	14.000	179.2936	5.2857	9.600	12.200	tss09	0.5753	1.03	405	-1.500	18.570
180.2408	31.5480	12.700	3.300	180.2490	31.5661	8.400	3.100	tss09	0.3299	1.16	331	4.300	4.528
180.4134	22.9419	-6.000	12.100	180.4348	22.9503	-25.200	11.700	tss09	0.2595	1.29	311	19.200	16.832
181.2180	29.4868	8.100	2.700	181.2207	29.5116	15.700	28.700	tss09	0.4383	1.50	511	-7.600	28.827
181.2219	11.4114	2.500	7.300	181.2311	11.3902	8.200	6.300	tss09	0.6342	1.38	568	-5.700	9.643
181.9476	28.6580	-2.500	12.100	181.9574	28.6771	9.300	11.300	tss09	0.8003	1.25	563	-11.800	16.556
182.9671	60.7411	38.400	4.000	182.9935	60.7393	37.600	2.500	tss09	0.6368	0.78	322	0.800	4.717
183.2824	42.0687	-32.300	17.100	183.2874	42.0426	23.700	12.800	tss09	0.7347	1.58	691	-56.000	21.360
183.4948	0.0990	19.600	17.700	183.4964	0.1291	18.200	12.000	tss09	0.5069	1.81	668	1.400	21.384

Table A2 continued

Table A2 (*continued*)

Source 1				Source 2									
RA1	Dec1	RM1	σ_{RM1}	RA2	Dec2	RM2	σ_{RM2}	Ref.	z	Δr	LS	ΔRM	$\sigma_{\Delta RM}$
(deg)	(deg)	(rad m $^{-2}$)		(deg)	(deg)	(rad m $^{-2}$)			(arcmin)	(kpc)	(rad m $^{-2}$)		
183.7011	3.0624	-1.200	5.100	183.7177	3.0686	21.400	5.900	tss09	0.6198	1.06	432	-22.600	7.799
183.7660	3.6750	-25.200	18.100	183.7903	3.6773	-0.900	5.100	tss09	0.4260	1.46	489	-24.300	18.805
184.0060	20.3604	-23.200	16.100	184.0375	20.3436	-20.600	10.000	tss09	0.4164	2.03	671	-2.600	18.953
186.1137	42.1029	-6.700	2.500	186.1219	42.1159	18.300	2.800	tss09	0.3918	0.86	274	-25.000	3.754
186.1535	23.9871	0.500	4.300	186.1712	23.9787	-4.200	10.700	tss09	0.6126	1.09	442	4.700	11.532
186.2657	12.8764	10.400	1.600	186.2696	12.8952	-9.200	4.800	tss09	0.0034	1.15	5	19.600	5.060
187.2753	31.6185	-5.700	6.300	187.2822	31.6341	-6.900	13.600	tss09	0.4982	1.00	366	1.200	14.988
188.6173	41.1650	-22.600	1.700	188.6351	41.1541	-26.300	2.600	tss09	0.1909	1.03	197	3.700	3.106
188.8457	21.3384	-6.800	4.900	188.8795	21.3476	-6.500	17.900	tss09	0.4227	1.97	657	-0.300	18.559
188.9032	-25.1906	-37.400	4.100	188.9116	-25.2174	-40.500	12.100	tss09	0.3552	1.67	500	3.100	12.776
189.2063	25.1263	4.800	7.300	189.2231	25.1344	21.200	13.300	tss09	0.5460	1.03	395	-16.400	15.172
189.2645	1.5982	2.900	10.000	189.2815	1.5993	-24.200	8.100	tss09	0.5195	1.02	381	27.100	12.869
189.5222	36.9264	-3.300	19.200	189.5232	36.9541	7.600	9.000	tss09	0.3154	1.67	462	-10.900	21.205
189.7798	5.3235	21.800	10.000	189.7971	5.3209	9.200	7.700	tss09	0.4590	1.04	364	12.600	12.621
189.8943	39.8595	-27.300	10.300	189.9157	39.8546	-17.600	13.200	tss09	0.7468	1.03	453	-9.700	16.743
190.3872	6.9337	5.000	5.000	190.3916	6.9480	10.200	6.900	tss09	0.6279	0.90	369	-5.200	8.521
190.4120	35.8961	5.900	15.600	190.4278	35.9004	25.700	17.900	tss09	0.6041	0.81	326	-19.800	23.744
191.1605	18.7393	38.400	2.900	191.1765	18.7396	34.100	6.600	tss09	0.2599	0.90	217	4.300	7.209
191.5083	25.8983	2.900	8.800	191.5553	25.8953	-0.800	21.700	tss09	0.5774	2.54	1001	3.700†	23.416
191.9778	46.1792	6.200	10.400	191.9963	46.1711	-0.300	15.100	tss09	0.5729	0.91	357	6.500	18.335
192.3457	22.6630	18.700	11.700	192.3587	22.6799	-5.700	8.200	tss09	0.5732	1.24	487	24.400	14.287
192.4532	33.3877	-5.500	1.900	192.4764	33.3918	-1.600	6.300	tss09	0.4627	1.19	418	-3.900	6.580
192.8196	18.1841	23.700	16.200	192.8395	18.1946	9.900	4.900	tss09	0.3446	1.30	382	13.800	16.925
192.9193	8.9329	10.600	1.000	192.9353	8.9411	14.300	2.800	tss09	0.0831	1.07	100	-3.700	2.973
193.9155	25.1438	22.400	15.000	193.9377	25.1113	7.200	15.300	tss09	0.4355	2.29	777	15.200	21.426
194.1006	55.4637	15.400	4.700	194.1043	55.4832	24.400	5.800	tss09	0.6478	1.18	490	-9.000	7.465
194.2142	2.3122	-17.900	4.700	194.2363	2.3219	-0.200	7.500	tss09	0.4864	1.44	520	-17.700	8.851
194.4805	4.9882	33.000	5.100	194.4843	4.9708	26.500	16.700	tss09	0.3882	1.07	339	6.500	17.461
195.1504	9.8158	17.100	3.400	195.1714	9.8237	14.800	3.100	tss09	0.6034	1.33	535	2.300	4.601
195.9475	7.9721	7.000	2.800	195.9597	7.9601	9.000	2.100	tss09	0.6610	1.02	427	-2.000	3.500
197.4702	51.5072	1.600	14.500	197.4836	51.5236	14.500	13.600	tss09	0.4845	1.11	400	-12.900	19.880
197.6442	59.9736	-5.000	14.900	197.6500	59.9878	-4.500	8.000	tss09	0.6738	0.87	367	-0.500	16.912
197.9266	40.9365	-7.200	3.600	197.9347	41.0277	-5.400	6.500	tss09	0.1103	5.49	663	-1.800	7.430
199.8915	2.8334	-2.100	7.700	199.9031	2.8423	-12.700	10.000	tss09	0.2922	0.88	231	10.600	12.621
200.1777	15.2790	8.500	17.300	200.1925	15.2866	-2.100	14.500	tss09	0.7491	0.97	427	10.600	22.573
200.2191	64.5544	59.200	17.600	200.2515	64.5640	9.700	4.700	tss09	0.2398	1.01	230	49.500	18.217
200.2547	58.5439	2.800	4.800	200.2736	58.5542	-0.700	6.500	tss09	0.0528	0.86	53	3.500	8.080
201.7676	-2.8330	19.800	7.600	201.7852	-2.8176	15.900	9.700	tss09	0.2392	1.40	318	3.900	12.323
201.8773	18.8868	-12.900	9.200	201.8866	18.9233	-9.000	7.100	tss09	0.6714	2.26	953	-3.900	11.621
202.1450	63.4797	-10.700	10.400	202.1752	63.4975	-4.300	9.400	tss09	0.2190	1.34	285	-6.400	14.019
202.6937	48.3509	-2.800	10.700	202.7156	48.3509	14.500	7.000	tss09	0.4366	0.87	296	-17.300	12.786
202.8149	23.9396	-17.300	13.100	202.8405	23.9619	-24.900	14.400	tss09	0.3361	1.94	560	7.600	19.467
202.8577	24.9984	-1.600	8.200	202.8706	25.0219	2.900	13.000	tss09	0.1517	1.57	249	-4.500	15.370
203.5391	55.0305	3.500	4.500	203.5604	55.0148	2.000	5.600	tss09	1.2473	1.19	595	1.500	7.184

Table A2 *continued*

Table A2 (continued)

Source 1				Source 2									
RA1	Dec1	RM1	σ_{RM1}	RA2	Dec2	RM2	σ_{RM2}	Ref.	z	Δr	LS	ΔRM	$\sigma_{\Delta \text{RM}}$
(deg)	(deg)	(rad m $^{-2}$)		(deg)	(deg)	(rad m $^{-2}$)			(arcmin)	(kpc)	(rad m $^{-2}$)		
203.5780	6.5683	-9.000	7.900	203.5824	6.5834	6.600	1.600	tss09	0.3974	0.94	302	-15.600	8.060
204.0583	49.0104	11.100	10.600	204.0743	48.9952	10.700	16.500	tss09	0.1092	1.11	133	0.400	19.611
204.0920	23.4711	1.600	3.200	204.0985	23.4889	4.800	3.400	tss09	0.1457	1.13	173	-3.200	4.669
204.4583	18.6371	5.600	3.800	204.4716	18.6453	6.800	3.600	tss09	0.1099	0.91	109	-1.200	5.235
205.3793	53.7515	-3.300	5.000	205.3995	53.7422	19.900	4.500	tss09	0.1997	0.91	180	-23.200	6.727
205.6972	8.5701	2.500	11.000	205.7290	8.5570	5.200	3.800	tss09	0.3930	2.04	651	-2.700	11.638
206.3758	62.1861	-21.400	10.600	206.4097	62.1835	-27.800	20.200	tss09	0.2294	0.96	211	6.400	22.812
206.9480	32.9672	20.100	15.300	206.9530	32.9815	2.900	13.400	tss09	0.4141	0.90	296	17.200	20.338
207.0869	28.5394	35.600	14.100	207.0963	28.5555	-2.300	2.800	tss09	0.5203	1.09	408	37.900	14.375
207.7885	7.4804	3.400	4.000	207.8032	7.4791	1.800	4.800	tss09	0.1501	0.88	138	1.600	6.248
208.2789	28.1469	15.900	5.600	208.2926	28.1579	17.900	9.200	tss09	0.4420	0.98	335	-2.000	10.770
209.1803	32.3218	-6.700	3.300	209.1926	32.3377	5.400	3.900	tss09	0.6472	1.14	473	-12.100	5.109
209.8668	-10.5415	4.800	12.500	209.8730	-10.5556	19.300	8.600	tss09	0.5207	0.92	344	-14.500	15.173
210.3865	-21.7076	-21.500	4.300	210.4002	-21.6953	-24.800	2.500	tss09	0.5000	1.06	388	3.300	4.974
210.7979	38.4729	-6.000	5.100	210.8011	38.4562	-6.000	5.600	tss09	0.5414	1.01	386	0.000	7.574
211.2786	16.2601	-12.900	15.200	211.2977	16.2695	-21.400	10.400	tss09	0.5840	1.24	491	8.500	18.417
211.3492	17.0023	-2.900	6.400	211.3500	17.0171	4.900	7.200	tss09	0.1702	0.89	155	-7.800	9.633
212.1895	31.4037	5.700	5.400	212.2061	31.4053	9.000	10.000	tss09	0.5536	0.86	332	-3.300	11.365
212.4967	31.4146	8.700	4.400	212.5200	31.4209	5.500	5.700	tss09	0.7039	1.25	537	3.200	7.201
212.6295	24.4757	-1.500	6.700	212.6324	24.4919	6.700	6.500	tss09	0.6283	0.98	402	-8.200	9.335
212.8972	-3.3388	-2.100	7.100	212.9012	-3.3169	-0.200	8.600	tss09	0.7237	1.34	582	-1.900	11.152
213.0660	43.6387	1.300	5.700	213.0797	43.6239	-8.700	4.400	tss09	0.6387	1.07	442	10.000	7.201
213.7198	22.6320	-2.800	13.600	213.7355	22.6354	21.900	13.300	tss09	0.1546	0.89	143	-24.700	19.022
214.6592	0.3957	21.100	13.200	214.6719	0.3998	2.900	7.700	tss09	0.7921	0.80	359	18.200	15.282
214.9334	8.2338	4.200	9.900	214.9572	8.2449	17.800	7.800	tss09	0.3210	1.57	440	-13.600	12.604
215.4173	10.2856	42.400	9.600	215.4385	10.2643	46.700	7.500	tss09	0.3739	1.79	554	-4.300	12.182
215.8613	-0.8324	-1.100	13.200	215.8650	-0.8125	-4.500	5.600	tss09	0.7106	1.21	522	3.400	14.339
216.0733	26.2229	4.100	9.200	216.0925	26.2299	-0.800	5.400	tss09	0.6767	1.12	474	4.900	10.668
216.1561	26.6245	0.800	4.600	216.1798	26.6244	14.600	14.200	tss09	0.0371	1.27	56	-13.800	14.926
216.9023	-12.0599	1.900	2.100	216.9136	-12.0674	-13.800	1.400	tss09	0.8029	0.80	361	15.700	2.524
218.6822	9.5247	-2.100	18.000	218.7026	9.4697	-1.200	7.600	tss09	0.6034	3.51	1412	-0.900†	19.539
220.6981	53.9031	9.300	3.700	220.7232	53.9190	17.800	8.800	tss09	0.5864	1.30	516	-8.500	9.546
221.4930	12.3746	14.500	6.300	221.5104	12.3830	11.600	6.800	tss09	0.5134	1.14	424	2.900	9.270
221.5973	41.5541	-1.500	4.000	221.6300	41.5568	-4.100	10.900	tss09	0.5351	1.48	562	2.600	11.611
221.9350	59.2962	10.000	14.000	221.9440	59.3136	-0.600	4.900	tss09	0.7777	1.08	482	10.600	14.833
222.3292	21.0967	11.900	3.700	222.3374	21.0827	12.000	2.800	tss09	0.2547	0.95	226	-0.100	4.640
222.7082	43.4904	-15.300	6.400	222.7233	43.5029	-14.200	2.100	tss09	0.6841	1.00	425	-1.100	6.736
223.4148	22.7241	22.200	15.800	223.4633	22.7169	20.900	15.700	tss09	0.3434	2.72	797	1.300	22.274
223.5422	44.5226	-13.500	15.400	223.5474	44.5375	7.400	10.800	tss09	0.6916	0.92	393	-20.900	18.810
223.6570	0.2811	34.900	4.900	223.6703	0.2950	30.000	3.800	tss09	0.5785	1.15	454	4.900	6.201
223.7556	-4.3618	7.300	5.800	223.7560	-4.3396	9.800	4.000	tss09	0.4410	1.33	455	-2.500	7.046
224.0084	16.4508	1.000	5.100	224.0339	16.4462	-0.200	4.300	tss09	0.2871	1.49	386	1.200	6.671
225.4834	7.8681	-2.700	2.600	225.4927	7.8788	1.300	3.100	tss09	0.6587	0.85	356	-4.000	4.046
226.4507	8.0856	12.900	9.100	226.4717	8.1022	17.700	10.900	tss09	0.4959	1.60	584	-4.800	14.199

Table A2 continued

Table A2 (continued)

Source 1				Source 2									
RA1	Dec1	RM1	σ_{RM1}	RA2	Dec2	RM2	σ_{RM2}	Ref.	z	Δr	LS	ΔRM	$\sigma_{\Delta RM}$
(deg)	(deg)	(rad m $^{-2}$)		(deg)	(deg)	(rad m $^{-2}$)			(arcmin)	(kpc)	(rad m $^{-2}$)		
227.5281	-1.5234	8.800	15.000	227.5352	-1.5111	-4.800	15.300	tss09	0.4536	0.85	295	13.600	21.426
227.7376	7.8569	1.300	5.600	227.7654	7.8734	25.300	12.700	tss09	0.4594	1.92	672	-24.000	13.880
227.8673	0.6145	-0.700	7.400	227.8834	0.5996	2.900	5.100	tss09	0.5225	1.31	491	-3.600	8.987
227.8791	32.4651	12.800	8.300	227.8809	32.4788	9.600	13.300	tss09	0.6529	0.83	346	3.200	15.677
228.0592	45.6930	-23.900	7.500	228.1114	45.6748	-31.600	18.700	tss09	0.3789	2.45	764	7.700	20.148
232.5213	23.2728	8.800	4.100	232.5441	23.2716	13.100	6.500	tss09	0.0899	1.26	127	-4.300	7.685
234.7095	20.1893	8.600	8.900	234.7280	20.1995	13.500	12.800	tss09	0.4849	1.21	436	-4.900	15.590
234.9838	48.5863	8.400	5.400	235.0069	48.6024	-4.000	8.300	tss09	0.0667	1.33	102	12.400	9.902
235.2572	59.2694	-2.200	6.200	235.2931	59.2601	-1.300	5.500	tss09	0.4671	1.23	434	-0.900	8.288
235.3638	34.1779	6.300	1.900	235.3715	34.1913	9.700	3.700	tss09	0.1273	0.89	122	-3.400	4.159
235.4218	-1.2401	10.200	12.800	235.4347	-1.2534	16.400	5.000	tss09	0.5666	1.12	437	-6.200	13.742
236.4702	11.5158	10.200	9.600	236.4857	11.5078	-12.500	9.300	tss09	0.4627	1.03	362	22.700	13.366
237.2700	26.7374	42.100	6.900	237.2754	26.7138	27.400	4.400	tss09	0.6162	1.45	589	14.700	8.184
237.3478	29.0939	20.700	13.700	237.3713	29.0962	8.300	9.900	tss09	0.7261	1.24	540	12.400	16.903
237.8235	42.6672	20.200	13.000	237.8294	42.6419	6.600	8.000	tss09	0.7836	1.54	689	13.600	15.264
237.9034	10.6063	34.200	18.400	237.9288	10.5903	51.300	8.400	tss09	0.3662	1.78	543	-17.100	20.227
238.4273	4.7127	13.300	9.400	238.4406	4.7071	4.600	10.600	tss09	0.4721	0.86	305	8.700	14.168
239.6956	1.8985	-2.100	6.500	239.7090	1.9188	29.800	12.900	tss09	0.5938	1.46	583	-31.900	14.445
240.1965	29.4848	8.000	8.100	240.1997	29.4970	5.200	5.400	tss09	0.5992	0.75	301	2.800	9.735
241.0553	32.3435	2.100	3.100	241.0564	32.3583	3.400	3.200	tss09	0.4525	0.89	309	-1.300	4.455
241.3045	7.1816	24.500	11.500	241.3106	7.2092	19.400	11.200	tss09	0.3112	1.69	463	5.100	16.053
242.0912	41.8964	16.700	14.800	242.0965	41.8767	35.600	10.600	tss09	0.2872	1.20	311	-18.900	18.204
242.5141	32.9789	-1.000	4.900	242.5323	32.9764	6.700	1.000	tss09	0.6275	0.92	377	-7.700	5.001
242.6542	6.0788	29.400	7.400	242.6583	6.0936	14.200	6.400	tss09	0.2408	0.93	212	15.200	9.784
244.4251	32.3688	-7.900	2.200	244.4303	32.3840	4.000	1.200	tss09	5.1902	0.95	351	-11.900†	2.506
244.7779	-3.0846	4.200	4.700	244.7918	-3.0673	-26.200	8.900	tss09	0.0688	1.33	105	30.400	10.065
245.0702	22.7403	56.400	14.700	245.0872	22.7554	32.000	15.100	tss09	0.2125	1.30	270	24.400	21.074
245.9904	47.3374	7.900	5.800	245.9941	47.3219	9.000	5.200	tss09	0.6500	0.94	391	-1.100	7.790
246.6475	-36.5579	34.200	5.900	246.6716	-36.5544	13.400	12.300	tss09	0.0432	1.18	60	20.800†	13.642
247.7748	5.0400	-12.300	14.800	247.7785	5.0220	-11.800	11.200	tss09	0.5263	1.10	414	-0.500	18.560
247.9146	-26.9458	-155.500	4.100	247.9324	-26.9494	-156.100	4.200	tss09	0.1660	0.97	166	0.600	5.869
249.7477	-9.9818	-231.100	6.800	249.7642	-9.9789	-225.000	7.100	tss09	0.6129	0.99	401	-6.100	9.831
250.1585	20.8837	47.100	7.400	250.1742	20.8854	42.100	9.000	tss09	0.3763	0.88	273	5.000	11.652
251.2129	37.5076	23.300	13.000	251.2303	37.4956	11.100	13.500	tss09	0.7583	1.10	487	12.200	18.742
251.3642	13.3631	37.900	1.800	251.3753	13.3790	32.600	3.600	tss09	0.5542	1.16	448	5.300	4.025
252.6401	16.7523	34.000	6.200	252.6540	16.7473	39.100	3.500	tss09	0.2829	0.85	218	-5.100	7.120
252.9123	-6.3124	36.000	12.400	252.9264	-6.2961	11.600	2.600	tss09	0.2360	1.29	290	24.400	12.670
254.8649	47.0536	9.100	1.400	254.8790	47.0403	14.100	0.900	tss09	0.2233	0.99	214	-5.000	1.664
256.2447	35.2956	5.100	10.400	256.2605	35.3042	-7.300	14.400	tss09	0.6650	0.93	391	12.400	17.763
256.2561	38.6773	12.800	2.300	256.2774	38.6771	10.500	3.400	tss09	0.4271	1.00	335	2.300	4.105
256.4883	77.1032	-18.900	7.200	256.5479	77.1233	-20.200	4.400	tss09	0.2040	1.44	290	1.300	8.438
257.2743	9.3950	24.900	10.000	257.2934	9.4059	41.300	4.000	tss09	0.0705	1.31	106	-16.400	10.770
258.8871	24.1727	78.600	14.500	258.9067	24.1868	68.100	8.500	tss09	0.4392	1.36	464	10.500	16.808
259.3406	43.9658	30.200	5.300	259.3632	43.9648	40.600	5.200	tss09	0.5422	0.98	375	-10.400	7.425

Table A2 continued

Table A2 (continued)

Source 1				Source 2									
RA1	Dec1	RM1	σ_{RM1}	RA2	Dec2	RM2	σ_{RM2}	Ref.	z	Δr	LS	ΔRM	$\sigma_{\Delta \text{RM}}$
(deg)	(deg)	(rad m $^{-2}$)		(deg)	(deg)	(rad m $^{-2}$)			(arcmin)	(kpc)	(rad m $^{-2}$)		
260.3330	25.8331	52.600	10.900	260.3490	25.8178	89.500	17.100	tss09	0.2331	1.26	281	-36.900	20.279
262.0747	31.7700	67.400	4.300	262.0940	31.7634	87.200	4.100	tss09	0.1665	1.06	181	-19.800	5.941
262.4773	45.0979	15.900	5.400	262.4927	45.1059	29.300	3.000	tss09	0.6673	0.81	341	-13.400	6.177
262.8542	25.9811	61.200	4.400	262.8712	25.9805	54.700	7.300	tss09	0.3587	0.91	274	6.500	8.523
263.1315	72.4230	-24.900	14.300	263.1713	72.4332	7.700	16.500	tss09	0.4154	0.94	310	-32.600	21.834
263.7559	29.6207	65.400	6.800	263.7733	29.6225	48.100	5.200	tss09	0.6004	0.91	365	17.300	8.560
264.2437	51.5424	13.100	16.300	264.2477	51.5291	16.300	5.500	tss09	0.5364	0.81	308	-3.200	17.203
265.3122	54.7406	12.800	3.400	265.3400	54.7311	-2.900	7.300	tss09	0.5322	1.12	424	15.700	8.053
272.8846	13.5814	95.800	7.600	272.8847	13.5673	107.400	6.600	tss09	0.4980	0.85	311	-11.600	10.066
295.6909	61.6814	79.300	4.200	295.7034	61.6631	70.900	5.500	tss09	0.7132	1.16	501	8.400	6.920
298.0545	2.5073	-34.300	3.800	298.0762	2.5083	-29.800	7.400	tss09	0.0590	1.30	89	-4.500	8.319
299.1484	-12.5846	-108.500	4.200	299.1658	-12.5922	-95.100	4.000	tss09	0.2085	1.12	229	-13.400	5.800
307.1860	-19.5879	-25.900	11.100	307.2017	-19.5699	-12.800	8.000	tss09	0.3656	1.40	427	-13.100	13.682
310.7681	-18.1921	-11.600	5.600	310.7702	-18.2049	-22.400	8.700	tss09	0.6904	0.78	333	10.800	10.346
310.9047	5.5197	82.100	11.200	310.9123	5.5327	71.400	12.800	tss09	0.3679	0.90	276	10.700	17.008
312.0521	-24.3380	5.700	9.200	312.0668	-24.3508	-17.000	2.100	tss09	0.7300	1.11	484	22.700	9.437
316.2248	-3.0469	10.900	12.700	316.2466	-3.0558	-29.200	18.700	tss09	0.4774	1.41	504	40.100	22.605
316.8038	23.5233	-162.200	12.600	316.8156	23.5323	-128.300	8.400	tss09	0.6051	0.84	338	-33.900	15.143
318.3778	4.7558	71.800	4.500	318.4029	4.7564	60.000	9.300	tss09	0.4072	1.50	489	11.800	10.332
320.2722	-14.7985	-1.500	12.400	320.2887	-14.7824	-12.800	10.700	tss09	0.2555	1.36	324	11.300	16.378
321.1401	-10.8291	-8.000	6.000	321.1451	-10.8438	-11.400	2.800	tss09	0.3675	0.93	285	3.400	6.621
323.0022	10.8926	-76.500	12.800	323.0130	10.9068	-49.300	6.600	tss09	0.5941	1.07	427	-27.200	14.401
323.7979	-0.8759	5.200	13.800	323.8125	-0.8820	16.200	3.100	tss09	1.6619	0.95	483	-11.000	14.144
324.2230	27.7469	-43.700	11.400	324.2420	27.7538	-38.900	10.000	tss09	0.5490	1.09	419	-4.800	15.164
326.9519	11.9571	-12.600	9.600	326.9712	11.9668	-22.400	10.800	tss09	0.6264	1.27	520	9.800	14.450
327.3146	19.6702	-22.400	25.400	327.3561	19.6852	-17.900	13.900	tss09	0.4671	2.51	886	-4.500	28.955
327.4245	10.8225	-3.900	12.600	327.4257	10.8356	-11.400	13.400	tss09	0.3867	0.79	250	7.500	18.393
327.8596	28.8404	-121.600	13.200	327.8670	28.8543	-115.200	19.400	tss09	0.6349	0.92	379	-6.400	23.465
329.2025	-1.4149	5.600	5.700	329.2061	-1.4402	5.600	12.200	tss09	0.4651	1.53	539	0.000	13.466
329.2314	-18.2228	7.900	1.300	329.2469	-18.2349	24.500	3.300	tss09	0.6680	1.14	480	-16.600	3.547
329.9380	17.6793	-9.100	15.500	329.9620	17.6877	-19.300	13.000	tss09	0.2462	1.46	339	10.200	20.230
331.3083	-30.5342	-7.400	15.800	331.3238	-30.5687	14.700	11.400	tss09	0.1248	2.22	298	-22.100	19.483
331.5403	15.5377	-54.300	5.000	331.5652	15.5363	-51.000	14.600	tss09	0.0906	1.44	146	-3.300	15.432
332.3336	-24.8998	1.300	4.500	332.3530	-24.8878	19.900	4.500	tss09	0.1592	1.28	211	-18.600	6.364
332.5803	27.7051	-120.300	8.100	332.5851	27.6906	-84.300	14.000	tss09	0.5030	0.90	331	-36.000	16.174
333.2408	9.3298	-29.800	3.000	333.2561	9.3348	-31.900	5.900	tss09	0.6212	0.96	391	2.100	6.619
333.6884	25.6081	-107.000	17.800	333.6983	25.6232	-89.700	14.400	tss09	0.3066	1.06	288	-17.300	22.895
333.7456	11.7057	-14.900	11.000	333.7520	11.6888	-14.700	11.500	tss09	0.6001	1.09	437	-0.200	15.914
334.3748	2.2252	-8.700	14.100	334.3858	2.2163	-25.900	7.200	tss09	0.6716	0.85	359	17.200	15.832
334.5436	19.5055	-10.000	24.800	334.5874	19.5572	-31.100	13.900	tss09	0.1096	3.97	477	21.100	28.430
334.9232	-20.3623	-18.000	10.900	334.9465	-20.3534	4.700	10.000	tss09	1.1480	1.41	697	-22.700	14.792
339.0253	25.4476	-78.800	6.500	339.0296	25.4336	-88.000	2.800	tss09	0.5812	0.87	344	9.200	7.077
339.0828	3.7432	16.300	12.300	339.0982	3.7458	-2.500	12.900	tss09	0.3822	0.94	295	18.800	17.824
340.2957	17.6495	-53.300	8.300	340.3080	17.6406	-55.200	10.000	tss09	0.1632	0.88	148	1.900	12.996

Table A2 continued

Table A2 (continued)

Source 1				Source 2									
RA1 (deg)	Dec1 (deg)	RM1 (rad m ⁻²)	σ _{RM1}	RA2 (deg)	Dec2 (deg)	RM2 (rad m ⁻²)	σ _{RM2}	Ref.	z	Δr (arcmin)	LS (kpc)	ΔRM	σ _{ΔRM}
340.6096	12.8199	-6.100	6.100	340.6104	12.8364	-24.600	9.100	tss09	0.6765	0.99	419	18.500	10.955
340.9853	26.3937	-81.900	8.200	341.0031	26.3943	-95.800	8.100	tss09	0.3589	0.96	289	13.900	11.526
341.3558	31.8581	-150.800	3.100	341.3750	31.8582	-146.200	8.200	tss09	0.5703	0.97	380	-4.600	8.766
345.3163	19.6684	-31.700	6.400	345.3292	19.6767	-41.800	1.300	tss09	0.4267	0.88	295	10.100	6.531
346.6203	15.9139	-5.300	7.300	346.6334	15.9622	4.900	5.100	tss09	0.4389	2.99	1019	-10.200†	8.905
347.9887	27.8398	-96.800	9.200	348.0037	27.8310	-82.700	8.000	tss09	0.4372	0.95	323	-14.100	12.192
348.2843	-31.9628	4.200	4.500	348.3037	-31.9651	11.800	3.500	tss09	0.3336	0.99	284	-7.600	5.701
350.9191	49.9893	-29.600	7.500	350.9379	49.9954	-29.300	7.700	tss09	0.5329	0.81	307	-0.300	10.749
351.2290	28.0575	-69.000	7.100	351.2598	28.0588	-67.000	2.700	tss09	0.5717	1.63	639	-2.000	7.596
351.6465	7.3971	-1.300	8.700	351.6466	7.4134	7.600	6.900	tss09	0.5911	0.98	391	-8.900	11.104
352.1411	-21.1012	5.000	2.000	352.1570	-21.0926	4.700	1.800	tss09	0.5800	1.03	407	0.300	2.691
353.9628	50.0509	-45.900	5.700	353.9987	50.0489	-51.300	6.900	tss09	0.0658	1.39	105	5.400	8.950
354.7238	-10.9973	7.800	10.700	354.7436	-10.9812	3.900	16.800	tss09	0.3619	1.52	461	3.900	19.918
355.2081	-28.8159	14.400	3.000	355.2163	-28.8023	20.200	4.000	tss09	1.1403	0.92	454	-5.800	5.000
357.5633	-21.9780	4.300	8.400	357.5642	-21.9633	-9.700	8.900	tss09	0.0550	0.88	56	14.000	12.238
357.8668	-23.2769	5.900	3.900	357.8682	-23.2924	6.800	4.600	tss09	0.9520	0.93	442	-0.900	6.031
358.4758	40.3021	-90.800	2.900	358.5005	40.2956	-81.600	6.700	tss09	0.5769	1.19	469	-9.200	7.301
358.8384	79.9314	2.200	10.700	358.8549	79.9119	13.700	1.700	tss09	1.3360	1.18	595	-11.500	10.834
358.9035	5.3774	-1.600	11.600	358.9182	5.3826	-2.700	8.800	tss09	0.4664	0.93	328	1.100	14.560
359.0255	-1.5182	-13.200	11.300	359.0283	-1.5421	6.900	13.600	tss09	1.0286	1.44	697	-20.100	17.682
359.3046	28.1723	-77.500	10.600	359.3140	28.1582	-81.200	10.300	tss09	0.7567	0.98	433	3.700	14.780
359.6436	27.9038	-85.300	2.200	359.6607	27.9161	-77.200	2.300	tss09	0.4115	1.17	384	-8.100	3.183
359.9281	20.6006	-29.500	5.200	359.9456	20.6041	-30.900	1.700	tss09	0.5746	1.01	397	1.400	5.471

We thank the referee for very careful reading and very detailed comments. The authors are supported by the National Natural Science Foundation of China (NNSFC No. 11833009, U2031115, 11988101), and the Key Research Program of the Chinese Academy of Sciences (Grant No. QYZDJ-SSW-SLH021), and also the Open Project Program of the Key Laboratory of FAST, NAOC, Chinese Academy of Sciences. This research has made use of the NASA/IPAC Extragalactic Database (NED) which is operated by the Jet Propulsion Laboratory, California Institute of Technology, under contract with the National Aeronautics and Space Administration.

REFERENCES

- Ahumada, R., Allende Prieto, C., Almeida, A., et al. 2020, ApJS, 249, 3, doi: [10.3847/1538-4365/ab929e](https://doi.org/10.3847/1538-4365/ab929e)
- Akahori, T., & Ryu, D. 2010, ApJ, 723, 476, doi: [10.1088/0004-637X/723/1/476](https://doi.org/10.1088/0004-637X/723/1/476)
- . 2011, ApJ, 738, 134, doi: [10.1088/0004-637X/738/2/134](https://doi.org/10.1088/0004-637X/738/2/134)
- Athreya, R. M., Kapahi, V. K., McCarthy, P. J., & van Breugel, W. 1998, A&A, 329, 809
- Banfield, J. K., O'Sullivan, S. P., Wieringa, M. H., & Emonts, B. H. C. 2019, MNRAS, 482, 5250, doi: [10.1093/mnras/sty3108](https://doi.org/10.1093/mnras/sty3108)
- Banfield, J. K., Schnitzeler, D. H. F. M., George, S. J., et al. 2014, MNRAS, 444, 700, doi: [10.1093/mnras/stu1411](https://doi.org/10.1093/mnras/stu1411)

- Becker, R. H., White, R. L., & Helfand, D. J. 1995, ApJ, 450, 559, doi: [10.1086/176166](https://doi.org/10.1086/176166)
- Bernet, M. L., Miniati, F., Lilly, S. J., Kronberg, P. P., & Dessauges-Zavadsky, M. 2008, Nature, 454, 302, doi: [10.1038/nature07105](https://doi.org/10.1038/nature07105)
- Blandford, R. D., & Rees, M. J. 1974, MNRAS, 169, 395, doi: [10.1093/mnras/169.3.395](https://doi.org/10.1093/mnras/169.3.395)
- Blasi, P., Burles, S., & Olinto, A. V. 1999, ApJL, 514, L79, doi: [10.1086/311958](https://doi.org/10.1086/311958)
- Böhringer, H., Chon, G., & Kronberg, P. P. 2016, A&A, 596, A22, doi: [10.1051/0004-6361/201628873](https://doi.org/10.1051/0004-6361/201628873)
- Bonafede, A., Feretti, L., Murgia, M., et al. 2010, A&A, 513, A30, doi: [10.1051/0004-6361/200913696](https://doi.org/10.1051/0004-6361/200913696)
- Bonafede, A., Vazza, F., Brüggen, M., et al. 2013, MNRAS, 433, 3208, doi: [10.1093/mnras/stt960](https://doi.org/10.1093/mnras/stt960)
- Broderick, J. W., Bryant, J. J., Hunstead, R. W., Sadler, E. M., & Murphy, T. 2007, MNRAS, 381, 341, doi: [10.1111/j.1365-2966.2007.12277.x](https://doi.org/10.1111/j.1365-2966.2007.12277.x)
- Carilli, C. L., & Taylor, G. B. 2002, ARA&A, 40, 319, doi: [10.1146/annurev.astro.40.060401.093852](https://doi.org/10.1146/annurev.astro.40.060401.093852)
- Clarke, T. E., Kronberg, P. P., & Böhringer, H. 2001, ApJL, 547, L111, doi: [10.1086/318896](https://doi.org/10.1086/318896)
- Clegg, A. W., Cordes, J. M., Simonetti, J. M., & Kulkarni, S. R. 1992, ApJ, 386, 143, doi: [10.1086/171000](https://doi.org/10.1086/171000)
- Condon, J. J., Cotton, W. D., Greisen, E. W., et al. 1998, AJ, 115, 1693, doi: [10.1086/300337](https://doi.org/10.1086/300337)
- Di Gennaro, G., van Weeren, R. J., Brunetti, G., et al. 2021, Nature Astronomy, 5, 268, doi: [10.1038/s41550-020-01244-5](https://doi.org/10.1038/s41550-020-01244-5)
- Domínguez-Fernández, P., Vazza, F., Brüggen, M., & Brunetti, G. 2019, MNRAS, 486, 623, doi: [10.1093/mnras/stz877](https://doi.org/10.1093/mnras/stz877)
- Donnert, J., Vazza, F., Brüggen, M., & ZuHone, J. 2018, SSRv, 214, 122, doi: [10.1007/s11214-018-0556-8](https://doi.org/10.1007/s11214-018-0556-8)
- Dreher, J. W., Carilli, C. L., & Perley, R. A. 1987, ApJ, 316, 611, doi: [10.1086/165229](https://doi.org/10.1086/165229)
- Fanaroff, B. L., & Riley, J. M. 1974, MNRAS, 167, 31P, doi: [10.1093/mnras/167.1.31P](https://doi.org/10.1093/mnras/167.1.31P)
- Farnes, J. S., O'Sullivan, S. P., Corrigan, M. E., & Gaensler, B. M. 2014, ApJ, 795, 63, doi: [10.1088/0004-637X/795/1/63](https://doi.org/10.1088/0004-637X/795/1/63)
- Farnes, J. S., Rudnick, L., Gaensler, B. M., et al. 2017, ApJ, 841, 67, doi: [10.3847/1538-4357/aa7060](https://doi.org/10.3847/1538-4357/aa7060)
- Feretti, L., Giovannini, G., Govoni, F., & Murgia, M. 2012, A&A Rv, 20, 54, doi: [10.1007/s00159-012-0054-z](https://doi.org/10.1007/s00159-012-0054-z)
- Ferrari, C., Govoni, F., Schindler, S., Bykov, A. M., & Rephaeli, Y. 2008, SSRv, 134, 93, doi: [10.1007/s11214-008-9311-x](https://doi.org/10.1007/s11214-008-9311-x)
- Garrington, S. T., Leahy, J. P., Conway, R. G., & Laing, R. A. 1988, Nature, 331, 147, doi: [10.1038/331147a0](https://doi.org/10.1038/331147a0)
- Giovannini, G., Bonafede, A., Feretti, L., et al. 2009, A&A, 507, 1257, doi: [10.1051/0004-6361/200912667](https://doi.org/10.1051/0004-6361/200912667)
- Goodlet, J. A., Kaiser, C. R., Best, P. N., & Dennett-Thorpe, J. 2004, MNRAS, 347, 508, doi: [10.1111/j.1365-2966.2004.07225.x](https://doi.org/10.1111/j.1365-2966.2004.07225.x)
- Govoni, F., & Feretti, L. 2004, International Journal of Modern Physics D, 13, 1549, doi: [10.1142/S0218271804005080](https://doi.org/10.1142/S0218271804005080)
- Govoni, F., Dolag, K., Murgia, M., et al. 2010, A&A, 522, A105, doi: [10.1051/0004-6361/200913665](https://doi.org/10.1051/0004-6361/200913665)
- Hammond, A. M., Robishaw, T., & Gaensler, B. M. 2012, ArXiv:1209.1438. <https://arxiv.org/abs/1209.1438>
- Han, J. L. 2017, ARA&A, 55, 111, doi: [10.1146/annurev-astro-091916-055221](https://doi.org/10.1146/annurev-astro-091916-055221)
- Han, J. L., Beck, R., & Berkhuijsen, E. M. 1998, A&A, 335, 1117
- Han, J. L., Manchester, R. N., Berkhuijsen, E. M., & Beck, R. 1997, A&A, 322, 98
- Heald, G., Braun, R., & Edmonds, R. 2009, A&A, 503, 409, doi: [10.1051/0004-6361/200912240](https://doi.org/10.1051/0004-6361/200912240)
- Hill, G. J., & Lilly, S. J. 1991, ApJ, 367, 1, doi: [10.1086/169597](https://doi.org/10.1086/169597)
- Jones, D. H., Read, M. A., Saunders, W., et al. 2009, MNRAS, 399, 683, doi: [10.1111/j.1365-2966.2009.15338.x](https://doi.org/10.1111/j.1365-2966.2009.15338.x)
- Joshi, R., & Chand, H. 2013, MNRAS, 434, 3566, doi: [10.1093/mnras/stt1277](https://doi.org/10.1093/mnras/stt1277)
- Kierdorf, M., Beck, R., Hoeft, M., et al. 2017, A&A, 600, A18, doi: [10.1051/0004-6361/201629570](https://doi.org/10.1051/0004-6361/201629570)
- Kim, K.-T., Tribble, P. C., & Kronberg, P. P. 1991, ApJ, 379, 80, doi: [10.1086/170484](https://doi.org/10.1086/170484)
- Kimball, A. E., & Ivezić, Ž. 2008, AJ, 136, 684, doi: [10.1088/0004-6256/136/2/684](https://doi.org/10.1088/0004-6256/136/2/684)
- Kimball, A. E., & Ivezić, Ž. 2014, in IAU Symposium, Vol. 304, Multiwavelength AGN Surveys and Studies, ed. A. M. Mickaelian & D. B. Sanders, 238–239
- Laing, R. A. 1988, Nature, 331, 149, doi: [10.1038/331149a0](https://doi.org/10.1038/331149a0)
- Lamee, M., Rudnick, L., Farnes, J. S., et al. 2016, ApJ, 829, 5, doi: [10.3847/0004-637X/829/1/5](https://doi.org/10.3847/0004-637X/829/1/5)
- Lazio, T. J., Spangler, S. R., & Cordes, J. M. 1990, ApJ, 363, 515, doi: [10.1086/169362](https://doi.org/10.1086/169362)
- Leys, C., Ley, C., Klein, O., Bernard, P., & Licata, L. 2013, Journal of Experimental Social Psychology, 49, 764, doi: [10.1016/j.jesp.2013.03.013](https://doi.org/10.1016/j.jesp.2013.03.013)
- Malik, S., Chand, H., & Seshadri, T. R. 2020, ApJ, 890, 132, doi: [10.3847/1538-4357/ab6bd5](https://doi.org/10.3847/1538-4357/ab6bd5)
- Mao, S. A., Gaensler, B. M., Havercorn, M., et al. 2010, ApJ, 714, 1170, doi: [10.1088/0004-637X/714/2/1170](https://doi.org/10.1088/0004-637X/714/2/1170)
- Miley, G., & De Breuck, C. 2008, A&A Rv, 15, 67, doi: [10.1007/s00159-007-0008-z](https://doi.org/10.1007/s00159-007-0008-z)
- Minter, A. H., & Spangler, S. R. 1996, ApJ, 458, 194, doi: [10.1086/176803](https://doi.org/10.1086/176803)
- Neronov, A., Semikoz, D., & Banafsheh, M. 2013, ArXiv:1305.1450. <https://arxiv.org/abs/1305.1450>
- Oppermann, N., Junklewitz, H., Robbers, G., et al. 2012, A&A, 542, A93, doi: [10.1051/0004-6361/201118526](https://doi.org/10.1051/0004-6361/201118526)

- Oppermann, N., Junklewitz, H., Greiner, M., et al. 2015, A&A, 575, A118, doi: [10.1051/0004-6361/201423995](https://doi.org/10.1051/0004-6361/201423995)
- O'Sullivan, S. P., Purcell, C. R., Anderson, C. S., et al. 2017, MNRAS, 469, 4034, doi: [10.1093/mnras/stx1133](https://doi.org/10.1093/mnras/stx1133)
- O'Sullivan, S. P., Machalski, J., Van Eck, C. L., et al. 2019, A&A, 622, A16, doi: [10.1051/0004-6361/201833832](https://doi.org/10.1051/0004-6361/201833832)
- O'Sullivan, S. P., Brüggen, M., Vazza, F., et al. 2020, MNRAS, 495, 2607, doi: [10.1093/mnras/staa1395](https://doi.org/10.1093/mnras/staa1395)
- Owen, F. N., Rudnick, L., Eilek, J., et al. 2014, ApJ, 794, 24, doi: [10.1088/0004-637X/794/1/24](https://doi.org/10.1088/0004-637X/794/1/24)
- Pedelty, J. A., Rudnick, L., McCarthy, P. J., & Spinrad, H. 1989, AJ, 97, 647, doi: [10.1086/115011](https://doi.org/10.1086/115011)
- Pentericci, L., Van Reeven, W., Carilli, C. L., Röttgering, H. J. A., & Miley, G. K. 2000, A&AS, 145, 121, doi: [10.1051/aas:2000104](https://doi.org/10.1051/aas:2000104)
- Pratley, L., Johnston-Hollitt, M., Dehghan, S., & Sun, M. 2013, MNRAS, 432, 243, doi: [10.1093/mnras/stt448](https://doi.org/10.1093/mnras/stt448)
- Pshirkov, M. S., Tinyakov, P. G., & Urban, F. R. 2015, MNRAS, 452, 2851, doi: [10.1093/mnras/stv1273](https://doi.org/10.1093/mnras/stv1273)
- . 2016, Physical Review Letters, 116, 191302, doi: [10.1103/PhysRevLett.116.191302](https://doi.org/10.1103/PhysRevLett.116.191302)
- Riseley, C. J., Galvin, T. J., Sobey, C., et al. 2020, PASA, 37, e029, doi: [10.1017/pasa.2020.20](https://doi.org/10.1017/pasa.2020.20)
- Ryu, D., Kang, H., Cho, J., & Das, S. 2008, Science, 320, 909, doi: [10.1126/science.1154923](https://doi.org/10.1126/science.1154923)
- Schnitzeler, D. H. F. M. 2010, MNRAS, 409, L99, doi: [10.1111/j.1745-3933.2010.00957.x](https://doi.org/10.1111/j.1745-3933.2010.00957.x)
- Simonetti, J. H., & Cordes, J. M. 1986, ApJ, 310, 160, doi: [10.1086/164672](https://doi.org/10.1086/164672)
- Stasyszyn, F. A., & de los Rios, M. 2019, MNRAS, 487, 4768, doi: [10.1093/mnras/stz1450](https://doi.org/10.1093/mnras/stz1450)
- Stil, J. M., Taylor, A. R., & Sunstrum, C. 2011, ApJ, 726, 4, doi: [10.1088/0004-637X/726/1/4](https://doi.org/10.1088/0004-637X/726/1/4)
- Stuardi, C., O'Sullivan, S. P., Bonafede, A., et al. 2020, A&A, 638, A48, doi: [10.1051/0004-6361/202037635](https://doi.org/10.1051/0004-6361/202037635)
- Taylor, A. R., Stil, J. M., & Sunstrum, C. 2009, ApJ, 702, 1230, doi: [10.1088/0004-637X/702/2/1230](https://doi.org/10.1088/0004-637X/702/2/1230)
- Taylor, G. B., & Perley, R. A. 1993, ApJ, 416, 554, doi: [10.1086/173257](https://doi.org/10.1086/173257)
- Vacca, V., Murgia, M., Govoni, F., et al. 2010, A&A, 514, A71, doi: [10.1051/0004-6361/200913060](https://doi.org/10.1051/0004-6361/200913060)
- van Weeren, R. J., de Gasperin, F., Akamatsu, H., et al. 2019, SSRv, 215, 16, doi: [10.1007/s11214-019-0584-z](https://doi.org/10.1007/s11214-019-0584-z)
- van Weeren, R. J., Röttgering, H. J. A., Brüggen, M., & Hoeft, M. 2010, Science, 330, 347, doi: [10.1126/science.1194293](https://doi.org/10.1126/science.1194293)
- Vazza, F., Brunetti, G., Brüggen, M., & Bonafede, A. 2018, MNRAS, 474, 1672, doi: [10.1093/mnras/stx2830](https://doi.org/10.1093/mnras/stx2830)
- Vernstrom, T., Gaensler, B. M., Rudnick, L., & Andernach, H. 2019, ApJ, 878, 92, doi: [10.3847/1538-4357/ab1f83](https://doi.org/10.3847/1538-4357/ab1f83)
- Wan, L., & Daly, R. A. 1996, ApJ, 467, 145, doi: [10.1086/177590](https://doi.org/10.1086/177590)
- Xu, J., & Han, J.-L. 2014a, Research in Astronomy and Astrophysics, 14, 942, doi: [10.1088/1674-4527/14/8/005](https://doi.org/10.1088/1674-4527/14/8/005)
- Xu, J., & Han, J. L. 2014b, MNRAS, 442, 3329, doi: [10.1093/mnras/stu1018](https://doi.org/10.1093/mnras/stu1018)
- Yates, M. G., Miller, L., & Peacock, J. A. 1989, MNRAS, 240, 129, doi: [10.1093/mnras/240.1.129](https://doi.org/10.1093/mnras/240.1.129)